Signal Transduction Through a DNA-Based T Cell Receptor

Marcus J. Taylor[1,,3,4], Kabir Husain[3], Zev J. Gartner[5],
Satyajit Mayor[3,4*], and Ronald D. Vale[1,2, 4*]

[1]Dept. of Cellular and Molecular Pharmacology and the [2]Howard Hughes Medical Institute, University of California San Francisco, USA; [3]National Centre for Biological Sciences, Bangalore, India, [4]HHMI Summer Institute, Woods Hole MA, [5]Dept. of Pharmaceutical Chemistry, University of California San Francisco, USA

* Address correspondence to: ron.vale@ucsf.edu, mayor@ncbs.res.in

T cells mount an immune response based upon the strength of the interaction between its T cell receptor (TCR) and peptide-loaded MHCs (pMHC) on an antigen-presenting cell. How T cells become activated by some pMHCs, but not others with slightly shorter bound times, remains an unanswered question. Here, we developed a finely tunable synthetic receptor-ligand system in which the extracellular domains of the TCR and pMHC were replaced with two short hybridizing strands of DNA. Remarkably, the T cell signaling response can discriminate between DNA ligands differing by a single base pair. Single molecule imaging reveals that ligated receptors with longer bound times promote the binding of more ligands nearby to create clusters; stable clusters of 2-4 ligated receptors then trigger receptor phosphorylation and signaling. These results reveal how T cells convert the bound time of an extracellular receptor-ligand interaction into a physical reorganization of molecules in the membrane and intracellular signaling.

The recognition of foreign antigens by T cells begins with a binding interaction between cell surface peptide-loaded MHC (pMHC) and the T cell receptor (TCR) expressed on the surface of T cells. Through genetic recombination, each T cell expresses a unique TCR with its own binding specificity[1]. Unlike many cell surface receptors that interact with a single or limited number of ligands, the TCR is presented with a vast number of different peptides loaded onto MHC molecules. Thus, central to the process of activating mature T cells is the ability of the TCR to transmit intracellular signals only in response to MHC loaded with higher affinity peptides and ignore the majority of low affinity pMHC interactions. Previous studies have implicated the lifetime of the TCR-pMHC interaction as a key determinant in discriminating between activating and non-activating pMHC molecules[2,3]. However, a mechanistic explanation of how the lifetime of an extracellular interaction is 'read out' and then converted to an intracellular signal is not well understood.

Taking a reductionist approach to this problem, we sought to engineer a simplified system in which the strength and properties of TCR-ligand interactions could be systematically varied, influences from other co-receptors eliminated[4], and immediate downstream signaling reactions monitored at the single-molecule level. A strategy for simplifying the six subunit

TCR (α, β, which bind pMHC, and CD3ε, δ, γ, ζ, which contain ITAMs motifs for the intracellular tyrosine phosphorylation[5]) was developed first by Irving and Weiss[6]. These investigators developed a single chain TCR consisting of the intracellular ITAMs from the CD3ζ chain fused to the extracellular domain of the unrelated transmembrane protein CD8; in response to anti-CD8 antibody, this chimeric antigen receptor (CAR) signals and activates T cells. Subsequently, CARs have been developed in which the extracellular domain consisted of a single chain antibody directed towards cancer antigens, and CAR-expressing T cells are being used with promising results in cancer immunotherapy[7]. While CARs are a powerful system for engineering and understanding T cell signaling, it is difficult to vary the affinity of CAR-ligands in a graded and predictable manner. To have better control of the ligand-receptor interaction, we reasoned that complementary DNA pairing would provide a suitable system. By varying the length and sequence of DNA ligand-receptor pairs, the binding strength can be varied in a predictable manner because of the well-understood free-energy and kinetics of hybridization of Watson-Crick base pairing[8].

Development and characterization of a DNA – Chimeric Antigen Receptor

Our nucleic acid-based synthetic TCR (DNA-CAR) consists of a ssDNA covalently reacted to an extracellular SNAP tag protein[9] that was fused to a transmembrane domain and intracellular CD3ζ chain (Fig. 1a). To avoid any potential signaling cross-talk with a native receptor, we expressed this DNA-CAR in a TCR negative Jurkat cell line (JRT3)[10]. To stimulate the DNA-CAR, we replaced the antigen-presenting cell with a planar supported lipid bilayer (SLB) functionalized with a freely diffusing CLIP protein covalently bound with a complimentary strand of ssDNA (Methods). T cells and APCs initially interact through adhesion molecules (e.g. ICAM-LFA1), which may also have signaling functions[11]. To enable our DNA-CAR T cells to adhere to the SLB without any co-stimulus, we made use of a synthetic DNA 'adhesion system' that de-couples adhesion from cell signaling[12] (Fig. 1a).

A high affinity pMHC-TCR leads to increased intracellular calcium, MAP kinase activation, re-organization of the actin cytoskeleton and the re-localization of transcription factors to the

nucleus[5,13,14]. To assess whether the DNA-based CAR is capable of transmitting similar intracellular signals upon ligand binding, we first tested a high affinity 16mer DNA base pair interaction (predicted off-rate of >7 hr, as estimated from computational analysis[15]). When these cells were plated on SLBs with a high ligand density of ~120 molecules per μm^2, we observed the rapid reorganization of ligand-bound receptors into submicron clusters that recruited the tyrosine kinase ZAP70-GFP and translocated centripetally from the periphery to the cell center (Fig. 1b; Movie S1). This receptor behavior is similar to that reported for antibody or pMHC activated TCR[16-18]. The majority (~65%) of the DNA-CAR T cells also signaled through the MAP kinase cascade, as indicated by strong phospho-ERK (pERK) staining of the nucleus (Fig. 1c); this response was comparable to that produced by the strong stimulus of phorbol myristate acetate (PMA) (Fig. 1c) and to that reported for TCR-pMHC in native T cells[19].

To examine the kinetics of signaling, we designed a system which cells could be triggered to signal in a synchronous manner after they were adhered to the SLB through the inert DNA-adhesion system. To achieve such temporal control, we designed non-complementary ssDNA for the ligand and receptor and then introduced an oligonucleotide that could hybridize to both receptor and ligand DNA and thus bridge the two together (Fig. 1d). Following the addition of this "trigger strand", the adhered cells spread rapidly (2-5 min), a result of the activation of actin polymerization (Fig. 1e and Extended Data Fig. 1b). Intracellular calcium also rose after ~1 min (Fig. 1f; Movie S2), and CD69, a TCR activation marker, was expressed on the cell surface at 4 hr (Extended Data Fig. 1d). The timing of these responses are similar to those reported previously[6]. Thus, the DNA-based CAR induces similar intracellular signaling responses to those described for T cells triggered through TCR and pMHC.

Next, we tested how signaling is influenced by the length and sequence of the DNA using automated microscopy and image analysis of pERK staining as a readout (Extended Data Fig. 2a,b)[20]. For these experiments, we used the direct hybridizing ligand-receptor pair (Fig. 1a), since the ligand concentrations on the SLB can be carefully controlled and varied (Methods). Compared to the 16mer oligo, ligand dose response curves of the 13mer and 12mer oligo ligands produced progressively weaker MAP kinase signaling (Fig. 2a, b). The 11mer did not

elicit a measurable pERK response above background, even at the highest ligand density. We then attempted to restore signaling to the 11mer by mutating adenine/thymine (A/T) base pairs to guanine/cytosine (G/C) base pairs, which increases the binding free energy of hybridization (Supplemental Table 1). Remarkably, a single A/T to G/C mutation converted the initial non-signaling 11mer receptor to one that could elicit a pERK response at high ligand densities, and each additional G/C mutation increased the potency of the DNA receptor (Fig. 2c).

Since theoretical models[21-23] and biochemical data[2,3] have suggested that the bound time of the TCR and pMHC plays a critical role in signaling, we directly measured the lifetime of individual DNA receptor-ligand interactions at the cell-SLB interface using single molecule total internal reflection fluorescence microscopy (TIRFM)[24] (Fig 2d, and Extended Data Fig. 3). The bound time of the ligand for the receptor displayed a roughly exponential distribution (Fig. 2d and Extended Data Fig. 3c, d), with an observed half-life of ~2 s for the non-activating 11mer and a half-life of ~19 s for the 11mer with three additional G/C bases (Fig. 2c). The much slower off-rate of the 16mer DNA ligand could not be determined accurately, since these measurements were limited by the rate of photobleaching (Extended Data Fig. 3d). Overall, the ligand bound times and the ligand densities on the SLB required for half-maximal responses are similar to those reported for TCR-pMHC in comparable bilayer activation experiments[24]. Collectively, these results clearly show that increasing the GC base pairing of the receptor results in a longer ligand-receptor interaction and that the T cell signaling response can distinguish between DNA receptor-ligand interactions with small difference in binding free energy (~1 kcal/mol, Supplemental Table 1).

Single molecule imaging of DNA-CAR phosphorylation

We next wanted to examine how the extracellular receptor-ligand bound time is translated into intracellular biochemistry, the first step being the phosphorylation of the ITAM domains of the DNA-CAR receptor. Phosphorylation of the ITAMs leads to the recruitment of the kinase ZAP70[25] which phosphorylates downstream targets. To measure phosphorylation of DNA-CAR in live cells in real time, we examined the recruitment of ZAP70-GFP from the cytosol to

receptor-ligand complexes by TIRFM (Fig. 3; Extended Data Figs. 4e,f and 5). We first used the 16mer at a ligand density of 0.1 molecules per μm^2, a density below the threshold required to elicit a pERK response. Under these conditions, single receptor-ligand binding interactions can be observed clearly (Fig. 3a; Extended Data Fig. 5a; Movie S3). However, surprisingly only ~6% of the ligand binding events (trackable for 30 s or more) led to detectable ZAP70-GFP recruitment, despite the long bound time of the ligand-receptor interaction (Fig. 3b). In these rare cases, ZAP70-GFP recruitment was transient and lasted less than ~20 sec (Fig. 3c). To rule out the possibility that the observed low kinase recruitment is due to nonfluorescent endogenous ZAP70 outcompeting ZAP70-GFP for binding to the ligated receptor, we repeated these experiments in the P116 ZAP70 null Jurkat cell line[26]; very similar results were observed (Extended Data Fig. 5b-d), confirming that ZAP70 is not efficiently recruited to single receptor-ligand complexes at low ligand densities. Collectively, these observations indicate that a long-lived ligand binding interaction *per se* is not sufficient to trigger receptor phosphorylation.

Since binding of the high-affinity 16mer ligand did not lead to stable receptor phosphorylation, we next wished to understand what additional events might be needed to initiate this first step in signaling. To answer this question, we performed single molecules studies at a 10-fold higher 16mer ligand density (16mer ligand density of 1 molecule per μm^2) a regime in which 20% of the cells generate a pERK response (Figure 3d) and the ligand density was still low enough to enable clear single molecule imaging. At 1 molecule per μm^2, single 16mer receptor-ligand pairs formed initially and then grew into small clusters on the membrane within a few minutes of cell contact with the SLB (Fig. 3d; Movie S4). By quantitating the fluorescence increase of these small receptor ligand clusters, we could estimate how many bound ligands were present in a cluster at the initial moment of ZAP70-GFP recruitment (Fig. 3d, Extended Data Fig. 4). This analysis revealed that ZAP70-GFP is recruited more efficiently to receptor clusters containing three or more ligand-receptor (~80%) than to single ligated receptors (~20%) (Fig. 3e). Furthermore, the bound time of ZAP70-GFP on a single ligated receptor was short (half-life of ~10 s, Fig 3f and example 3 in Extended Data Fig 5a), as reported for at the lower ligand density on the bilayer (Fig. 3c). In striking contrast, nearly half of ZAP70-GFP molecules (48%) remained associated with small receptor clusters for 100 s or more (Fig. 3f). Thus, clusters composed of a just few bound receptors become phosphorylated and stably

recruit ZAP70-GFP, whereas single ligated receptor only occasionally and transiently bind ZAP70-GFP.

Comparison of low and high affinity ligands

We next sought to compare the behaviors of a low affinity (13mer DNA strand) and high affinity receptor (16mer) receptor interacting with their cognate ligands at the same density on supported lipid bilayer (1 molecule per μm^2). At this ligand density, at which only the higher affinity 16mer elicits a pERK response (Fig 2b), the two receptors showed considerable differences in their ability to form clusters. In the case of the 16mer, many (5-20) receptors clusters formed within a few minutes of cells landing on the bilayer (Fig 4a), and many of these clusters were long-lived (44% persisting for >100 s, Fig. 4b). During the same period of time with the 13mer ligand, single ligand-receptor binding events were observed but cluster formation was very rare. A few small clusters of ligated 13mer receptors began to appear on the cell surface after 15 min (Fig 4a), but most of these clusters disassembled rapidly (mean half-life of ~21 sec; Fig 4c, Movie S6). As described earlier for the 16mer ligand, ZAP70-GFP recruitment was observed with approximately 50% for clusters of three or more 13mer ligands and infrequently (~2%) observed with single receptor-ligand complexes (Extended Data Fig. 7b). Since the receptors clusters were transient, correspondingly, ZAP70-GFP also dissociated from the membrane (Extended Data Fig. 7b). Background fluorescence precluded single molecule measurements of the 13mer at ten-fold higher ligand densities on the bilayer. In summary, at the same ligand density of 1 molecule per μm^2, only the higher affinity receptor forms clusters and stably recruits ZAP70, which correlates with its ability to generate a rapid downstream pERK signaling response (Fig. 2b).

Mechanism of receptor-ligand cluster formation

We anticipated that receptor-ligand clusters might form through collisions between ligated receptors that are passively diffusing or actively being moved by the actin cytoskeleton in the plane of the plasma membrane. However, such collisions and fusions between single ligated receptors were rarely observed. More commonly, a single receptor-ligand complex grew in

fluorescence intensity in roughly quantized steps (Fig. 5a; Movie S4 and S7). This result is best explained by new ligand binding events occurring near to (within the diffraction limit boundary) pre-existing receptor-ligand complexes. We quantified the rate of new ligand-receptor binding events occurring adjacent to a pre-existing receptor-ligand (using an area of a diffraction-limited spot) versus the rest of the plasma membrane (area of the total cell footprint on the SLB as observed in the TIRFM field, Fig. 5b). This analysis revealed that the area-normalized on-rate is at least 550-fold higher near pre-existing bound receptor-ligand pairs or small clusters compared to the rest of the membrane (Fig. 5b). We observed a similar phenomenon of an enhanced ligand binding rate at pre-existing bound receptor-ligand complex in cells treated with latrunculin to depolymerize actin, although the magnitude of the effect was diminished (75-fold enhancement; Extended Data Fig. 8). After small clusters formed, we observed that they diffused and could sometimes fused with one another to form larger sized clusters (Fig. 5a; Movie S7). Thus, our results suggest that clusters develop primarily through an increase in the on-rate of ligand binding but also can grow in size by fusion events.

Discussion

In summary, our data show that the binding energy of extracellular DNA hybridization can be transduced across the plasma membrane to trigger intracellular phosphorylation of a chimeric antigen receptor and downstream MAP kinase signaling. We also show that longer bound-time of the DNA-CAR with its ligand and higher ligand densities on the bilayer synergize to promote receptor clustering and that the formation of long-lived receptor clusters substantially increases the probability of receptor phosphorylation and ZAP70-GFP recruitment compared with single ligated receptors. These results are consistent with statistical analysis indicating that the small clusters of ligated pMHC-TCR activate downstream calcium signaling[27].

Like many prior studies with different pMHC ligands interacting with TCR[18,28,29], we show that T cells can discriminate between different DNA ligands that have relatively small differences (a few fold) in receptor-bound times (Fig. 2d). A theory of "kinetic proofreading" was developed

to explain how relatively small differences in receptor bound time might be discriminated and lead to more binary downstream outputs[21]. In the general formulation of kinetic proofreading, signaling is triggered by a linked set of reactions that require the continuous occupancy of the ligand-receptor complex; if the ligand dissociates, then these reactions can be rapidly reversed. Many different molecular mechanisms have been put forth for the kinetic proofreading steps, including enzymatic reactions (e.g. phosphorylation)[21,30,31], receptor conformational changes[32,33], and receptor dimerization/oligomerization[34,35]; however, direct evidence is lacking and it also remains unclear whether kinetic proofreading occurs at the level of the receptor and/or farther downstream[24,36]. Our results provide direct evidence for spatial organization of receptors in kinetic proofreading by demonstrating that the initial receptor-ligand complex has very low signaling activity and must be converted to a cluster for robust phosphorylation and that cluster formation is readily reversible for lower affinity ligands. We show that the conversion of single receptor-ligand complexes to clusters is driven primarily by new receptor-ligand binding events occurring preferentially in their vicinity. Since the rate of formation of bi-molecular complexes is both time- and concentration-dependent, cluster growth is favored with longer dwell times of the initial ligand-receptor binding event and higher ligand concentrations, as we have observed. Additional time-dependent and reversible steps no doubt contribute to kinetic proofreading, which could include stabilizing the receptor-ZAP70 clusters themselves (Fig. 4a) and other downstream responses involving ERK[19]. The mechanism behind the dramatic acceleration of the ligand on-rate near to pre-existing ligand-receptors is not established. However, this phenomenon might arise from the closer physical proximity of the two membranes established by an initial receptor-ligand interaction[37,38] (Fig. 5c). Unbound receptors and ligands on opposite membranes that diffuse into zones of close contact could interact more readily compared to in regions where the two membranes are further apart and might require membrane fluctuations to bring them into a range where the receptor and ligand can interact[39,40]. In addition to promoting more ligand-receptor binding events, the zone of close membrane contact may exclude the transmembrane phosphatase CD45 and thus shift equilibrium reaction between the receptor kinase (Lck) – phosphatase (CD45) to favor net receptor phosphorylation ("kinetic segregation" model[41]). Exclusion of the transmembrane phosphatase CD45 has been observed for receptor clusters composed of many tens or hundreds of molecules[16,38]. However,

if CD45 exclusion underlies receptor phosphorylation, then this study suggests that clusters as small as even 2-4 receptors (whose expected diameters are well below the diffraction limit of light) can create physical zones that partially limit access of the CD45 phosphatase to its substrate (Fig. 5c).

The simple single-chain receptor (DNA-CAR) used in this study has allowed us to isolate and dissect early events in receptor signaling. The bound times of the 11mer and 13mer DNA receptor-ligands are comparable to the many TCR-pMHC complexes that have been extensively studied (few to tens of seconds[29]); and downstream signaling is elicited with ligand densities of (10-100 molecules per μm^2), which are comparable to those used to stimulate native T cells on supported lipid bilayers[18,27]. However, in the more physiological context of the APC-T cell conjugate, T cells respond to lower levels of pMHC[36,42]. In these contexts T cell signaling likely involves other components, such as additional phosphorylation sites from other TCR subunits (e.g. the CD3ε, δ, γ chains[5]), force-induced mechanical changes in the TCR[43], adhesion molecules that also form signaling complexes (e.g. LFA-1-ICAM1)[44], and numerous other co-receptors that enhance signaling (e.g. CD4/8, CD28-B7, CD2-CD58)[45]. In future work these additional components can be added to the DNA-CAR system to understand how they affect the assembly and phosphorylation kinetics of receptor clusters as well as influence downstream biochemical events that lead to T cell activation.

Acknowledgments:

We thank J. James (LMB and Cambridge University) for initial help and guidance with this project. We thank Sam Lord and Dyche Mullins for use of their microscope. We thank N. Stuurman for assistance with microscopy, C. Carbone for advice and assistance with experimental work, Noel Gee for supplying lipid-modified DNA, and E. Hui, J. Wilhelm and X. Su for comments on the manuscript. Some Image acquisition was performed at the Nikon Imaging Center at the University of California San Francisco, and at the NCBS (Bangalore). R.D.V. is a Howard Hughes Medical Institute investigator. MJT was supported by an AXA Postdoctoral Fellowship and NCBS campus fellowship. SM was supported by HFSP

RGP0027/2012, JC Bose Fellowship, and a Wellcome Trust DBT-Alliance Margadarshi Fellowship (SM).

Methods

Data Reporting

No statistical methods were used to predetermine sample size. The experiments were not randomized. The investigators were not blinded to allocation during experiments and outcome assessment. For outcome assessment of phosphoERK activation (see below, Fig. 2 and Extended Data Fig. 2), ligand-receptor cluster assembly and ZAP70 recruitment (see below, Fig. 3 and Extended Data Fig. 4) experiments were automatically analyzed by Cell Profiler or MATLAB scripts to minimize potential human bias.

Generation of DNA Chimeric Antigen Receptor and ZAP70 constructs

Two versions of the DNA-CAR were constructed: 1) DNA-CAR with a C-terminal cytoplasmic monomeric eGFP (herein termed "GFP") (pHR-DNA-CAR-GFP), and 2) a non-fluorescent alternate version with a N-terminal HA epitope tag (YPYDVPDYA). The HA tag was inserted to allow cell surface expression levels to be monitored via FACS. Full details of the construction of the DNA-CAR are given in supplemental methods and the oligonucleotides sequences used in cloning are listed in Supplementary Table 1. pHR-ZAP70-GFP and pHR-ZAP70-mCherry were as described earlier[38].

Cell Culture and Reagents

JRT3 Jurkat cells (which fail to express the TCR[10]) and P116 Jurkat cells (which do not express ZAP70[26]) were kindly provided by Art Weiss (UCSF). JRT3 Jurkat cells were confirmed to be TCR negative by FACS analysis. Both cell lines were grown in RPMI (Invitrogen) with 10% FBS (Invitrogen) supplemented with 2 mM L-glutamine. HEK-293T cells (purchased from the ATCC collection) were grown in DMEM (Invitrogen) supplemented with 2 mM L-glutamine. All cells were determined to be negative for mycoplasma using the MycoAlert detection kit (Lonza).

Lentiviral Production and Generation of Stable Expressing JRT3 Cell Lines

Lentivirus particles were produced in HEK-293T cells by co-transfection of the pHR transfer plasmids with second generation packaging plasmids pMD2.G and psPAX2 (a gift from Didier Trono, Addgene plasmid # 12259 and # 12260). Virus particles were harvested from the supernatant after 48-72 hr, filtered and applied to JRT3 cells overnight. The next day the cells were resuspended in fresh RPMI media and recovered for 3 days. DNA-CAR-GFP expressing JRT3 cells were FACS sorted to generate a stable and homogenous expressing population. JRT3 transduced with pHR-DNA-CAR-IRES-puro were selected at 4 μg/ml of puromycin (Sigma) and maintained with 2 μg/ml of puromycin.

Imaging Chambers and Supported Lipid Bilayers

Phospholipid mixtures consisting of 97.5% mol 1-palmitoyl-2-oleoyl-*sn*-glycero-3-phosphocholine (POPC), 2% mol 1,2-dioleoyl-sn-glycero-3-[(N-(5- amino-1-carboxypentyl) iminodiacetic acid) succinyl] (nickel salt) (Ni^{2+}-NTA-DOGS) and 0.5% mol 1,2-dioleoyl-sn-glycero-3- phosphoethanolamine-N-[methoxy(polyethylene glycol)-5000] (PE-PEG5000) were mixed in glass vials and dried down under argon. All lipids used were purchased from Avanti Polar Lipids. Dried lipids were placed under vacuum for 2 hr to remove trace chloroform and resuspended in PBS. Small unilamellar vesicles were produced by several freeze-thaw cycles. Once the suspension had cleared, the lipids were spun in a bench top ultracentrifuge at 65,000xg for 45 min and kept at 4° C for up to 5 days.

Supported lipid bilayers were formed in 96-well glass bottom plates (Matrical), which were cleaned by extensive rinsing in isopropanol following by water. Plates were then cleaned for 15 min with a 1% Hellmanex solution heated to 50°C followed by extensive washing with pure water. 96 well plates were dried with nitrogen and sealed until needed. To prepare SLB, individual wells were cut out and base etched for 5 min with 5 M KOH and then washed with water and finally PBS. SUVs suspension were then deposited in each well and allowed to form for 1 hr. We found that SUVs suspension containing 0.5% mol PE-PEG5000 formed best at 37°C. After 1 hr, wells were washed extensively with PBS. SLBs were incubated for 15 min with HEPES buffered saline (HBS: 20 mM HEPES, 135 mM NaCl, 4 mM KCl, 10 mM glucose, 1 mM $CaCl_2$, 0.5 mM $MgCl_2$) containing 1% BSA to block the surface and minimize non-specific protein adsorption. After blocking, the SLB were functionalized by incubation for 1 hr with his-

tagged proteins. The labeling solution was then washed out and each well was completely filled with HBS with 1% BSA. Total well volume was 625 µl (manufacturers specifications), and 525 µl was removed leaving 100 µl of HBS 1% BSA in each well.

Protein Expression, Purification and Labeling

SNAPf and CLIPf open reading frames were cloned into a pET28a vector containing a N-terminal 10X His tag. A C-terminal ybbr13 tag (DSLEFIASKLA)[46] was added by PCR. Proteins were expressed in BL21-DE3 E. coli and purified by Ni-NTA resin followed by gel filtration. Ybbr13 peptide labeling was performed using CoA-Atto647N as described[46]. The degree of labeled was calculated with a spectrophotometer by comparing 280nm and 640nm absorbance (usually 85%-95% labeling efficiency was achieved).

Synthesis of Benzylguanine-Conjugated DNA Oligonucleotides

All receptor/ligand/adhesion oligonucleotides were ordered from IDT with a 3'/5' terminal amine. Conjugation to benzyl-guanine or benzyl-cytosine was performed as described [47]. 10x His tagged SNAP and CLIP were labeled with benzlyguanine/benzylcytosine DNA on the same day SLBs were prepared. SNAP/CLIP were labeled at a concentration of 5 µM with a 3-fold excess of BG/BC-DNA in 20 mM HEPES (pH 7.4) 200 mM NaCl and 1 mM TCEP. DNA-SNAP/CLIP linkage was monitored by mobility shift assays using SDS-PAGE. Maximal labeling was achieved after 40 min at room temperature (~90% labeling efficiency).

DNA Ligand and Receptor Sequence Design

We selected a 16-nucleotide DNA strand that had no discernable secondary structure (as measured using nupack.org[15], accessed between 12/2012 and 06/2013) and have been previously characterized[48]. The receptor/ligand 16mer DNA strand had the following sequences: ligand (5′-CCACATACATCATATT-3′) and receptor (5'-AATATGATGTATGTGG-3'). All receptor/ligand DNA strands were ordered from Integrated DNA Technology with 3' amine functional group. Truncations of the initial 16mer DNA ligand sequence were generated from the 5' end. To maintain the overall length of the DNA ligand as presented on the SLB, a poly-thymine spacer was added back at the 3' end. The truncation ligands had the following sequence: 13mer ligand (5'- CATACATCATATTTTT-3'), 12mer ligand (5'-

ATACATCATATTTTTT-3'), and 11mer ligand (5'- TACATCATATTTTTT-3'). For experiments using shorter complementary DNA ligands the same 16mer DNA receptor sequence was used (5'-AATATGATGTATGTGG-3'). Mutant versions of the 11mer were generated by sequential addition of C/G base pairs. Mutant 11mer strands were analyzed by nupack.org to minimize secondary structure. The following mutant 11-nucleotide DNA receptor ligand pairs were used (mutations underlined): DNA receptor (5'-AATGTGATGTATTTTT-3'), DNA ligand (5'-TACATCACATTTTTTT-3'), DNA receptor (5'-AAGGTGATGTATTTTT-3'), DNA ligand (5'-TACCTCACCTTTTTTT-3') and DNA receptor (5'- AAGGTGAGGTATTTTT-3'). The triggerable DNA signaling system used the same 16mer DNA receptor (5′-CCACATACATCATATT-3). The SLB was functionalized with 18mer non-complementary oligonucleotide (5'-CCCTCATTCAATACCTCA-3'). Receptor and ligand were brought together by the addition of an oligo with complementary regions to both receptor and ligand (5'-AATATGATGTATGTGGttCCTAGGGTATTGAATGAGGG-3'). The addition of trigger strand results in a 34 base pair overlap. While this trigger strand system was useful for investigating kinetics by synchronizing the timing of ligand-receptor interaction, the complexity of this three-component binding interaction system[49] made it difficult to use for generating ligand dose responses.

DNA-Based Adhesion System

The 100mer adhesion strand used in this study consisted of a 3' 20mer complementary region (5'- ACTGACTGACTGACTGACTG-3') attached through a 80mer poly-dT linker to a lipid anchor (1,2-O-Dihexadecyl-sn-glycerol) via a phosphodiester linkage at the 5' end. Dialkylglycerol phosphoramidites were synthesized as previously described[12,50]. The complementary sequence (5'- CAGTCAGTCAGTCAGTCAGT-3') was ordered from Integrated DNA Technology with a 5' amine and labeled with BG-NHS as previously described above. This strand was then conjugated to His10-SNAPf to label SLBs. Cells were labeled with the DNA adhesion lipid molecule for 3 min at room temperature at a labeling concentration of 5 mM (stock concentration of 250 mM).

BG-DNA Labeling of JRT3 Cells Expressing DNA-CAR

JRT3 cells expressing DNA-CAR were spun down, re-suspended in HBS and incubated with 5 μM of BG-DNA receptor for 30 min at room temperature. Cells were conjugated with BG-DNA at an approximate density of 2 x 10^7 cells/ml. During conjugation cells were maintained in suspension by gently agitation. DNA adhesion lipid was added during the final 3 min of labeling. Cells were washed twice in HBS before being used.

CD69 Expression

To assay CD69 expression by FACS, supported lipid bilayer were set up on 7 μm silica beads (Bangs Laboratories). Silica beads were counted using a hemocytometer mixed with 2.5 x 10^5 JRT3 cells expression DNA-CAR-GFP in 96 well plates in a 3:1 ratio of bead to cells. Signaling was initiated by the addition of DNA trigger strand. A portion of cells were also plated onto poly-L-lysine containing coverslips and analyzed by spinning disk confocal to inspect SLB quality and confirm cellular activation via re-localization of DNA-CAR-GFP to the bead-cell interface after addition of the trigger DNA strand (Extended Data Fig. 1C). 4 hr after activation cells were pelleted and re-suspended in PBS with 2% (v/v) fetal bovine serum and 0.1% (w/v) NaN_3. Cells were labeled with mouse anti-CD69 conjugated to Alexa647 (FN50, Thermo Fisher Scientific, 10 μg/ml) for 1 hr on ice. Cells were washed twice and then fixed. Cells were then run on a LSRII (Becton Dickinson) (10,000 gated cells analyzed).

Calcium Imaging and Analysis

Calcium signaling assay was performed on JRT3 cells pre-incubated with 10 μM Fura-2 (Invitrogen) for 30 min. Ratiometric Fura-2 imaging (340 nm/380 nm excitation) was performed on a microscope (Nikon TE2000U) equipped with wavelength switcher (Sutter Instrument Co. Sutter Lambda XL lamp) and Fura-2 excitation and emission filters. Images were projected on to Photometric CoolSNAP HQ2 CCD camera using an S Fluor 40X 1.3 NA oil objective. JRT3 cells expressing DNA-CAR-GFP were pipetted onto supported lipid bilayer incubated for 10 min to allow cells to settle and adhere to the SLB using the DNA adhesion system described. Cells were imaged for 1-2 min in a quiescent state before the addition of trigger strand to initiate signaling. Image analysis was performed in FIJI[51] by manually

segmenting the cell outline and measuring the mean 340 nm/380 nm excitation ratio in the cell volume.

PhosphoERK Data Acquisition and Analysis

Titrations of ligand density on SLBs were set up using 96 well plates. For each phosphoERK assay, all SLB ligand densities were set up in triplicate. Ligand density was determined by maintaining identical labeling protein concentrations and time, but changing the portion of DNA-ligand labeled His10-CLIPf-Atto647N. Before application of cells, SLBs were analyzed by TIRFM to check formation, mobility and uniformity. Short time series were collected at low ligand densities (e.g. ≥1 molecule per μm^2) to calculate ligand densities on the SLB based upon direct single molecule counting. Wells containing only DNA adhesion strands served as unstimulated controls or used for phorbol 12-myristate 13-acetate stimulation.

On the day of an experiment JRT3 cells expressing DNA-CAR-GFP were transferred to serum free media for several hr before being functionalized with BG-DNA receptor. After DNA functionalization cells were re-suspended in HBS at a final concentration of 2.5×10^5 cells per ml. 100 µl of cells (corresponding to 2.5×10^4 cells per well) were then applied to 96 plates wells using a multichannel pipette (total well volume after addition of cell was 200 µl). Cells were then incubated at 37°C for 15 min before the addition of 200 µl of 2x fixative (7% (v/w) PFA with 1% (v/w) Triton X). Cells were fixed for 20 min at room temperature. Cells were then washed with PBS containing 60 mM glycine to quench PFA. Cells were then blocked in PBS 10% (w/v) BSA for 1 hr before addition of primary antibody. Cells were labeled over night with anti-phosphoERK (rabbit polyclonal, Cell Signalling Technology #9101, used at 1:500). The next day cells were washed 5X in PBS 10% (w/v) BSA, and labeled with goat anti-rabbit conjugated to Alexa555 (Invitrogen, used at 1:1000) for 1 hr. Finally cells were washed 5X in PBS. In the penultimate PBS wash, cells were labeled for 10 min with DAPI at a labeling concentration of 300 nM.

96 well plates were imaged on an inverted microscope (Nikon TiE, Tokyo, Japan) equipped with Lumencor Spectra-X illumination. Fluorescent images were acquired with Nikon plan apo 20X 0.75 NA air objective lens and projected on an Andor Zyla 5.2 camera with 2x2 binning

(pixel size 425nm) and a 1.5x magnification lens. The fluorescent emission was collected through filters for EGFP (525 ± 30nm), Alexa 555 (607 ± 36nm) and DAPI (440 ± 40). Image acquisition was performed using MicroManager software[26,52]. Each well was imaged using the Create Grid plugin in the MicroManager multidimensional acquisition GUI. The Create Grid plugin was used to automate the acquisition of the entire well. A dark image was subtracted from each image during acquisition using the Multi-channel shading MicroManager plugin.

Image analysis was performed using Cell Profiler[20] and FIJI. Unsuitable images that had focus defects or fluorescent debris were discarded from the image series from each well. The Alexa555 channel, corresponding to the phosphoERK staining, was processed in FIJI using the roll ball background subtraction (ball size 100 pixels) to create a background image. Background images from multiple fields of views were averaged to create an image of the illumination function of the microscope. Each Alexa555 image was then divided by this illumination image using the Cell Profiler plugin 'Correct illumination apply' to correct for illumination defects.

To score phosphoErk positive cells, selected phosphoERK and DAPI images from individual wells were processed in batch using a custom Cell Profiler pipeline. The DAPI channel was segmented to identify cell nuclei. The segmented nuclei were used to seed a second segmentation of the phosphoERK stained channel (Extended Data Fig. 2a). Thresholding parameters for the phosphoERK channel were set using images of PMA stimulated cells, unstimulated cells, and cells labeled with secondary only (for background fluorescence). Segmented nuclei were then related to the segmented phosphoERK objects to score nuclei as phosphoERK positive or negative (e.g. nuclei associate with or without a phosphoERK object). Due to the presence of small phosphoERK positive foci in a portion of cells (found in a fraction of cells even without ligand stimulation), we stipulated that phosphoERK segmented object had to have a minimum size (a minimum diameter of 20 pixels, Extended Data Figure 2a). This selected for a phosphoERK staining that had an equivalent size and morphology to the DAPI stain, and was equivalent to the phosphoERK staining morphology of PMA-stimulated cells. In general, between 2500-5000 cells were analyzed per well. Positive and negative phosphoERK nuclei were summed across images from the same well.

Imaging and analysis of single ligand-receptor dwell time

Single molecule measurements of receptor ligand dwell time were performed on an inverted microscope (Nikon TiE,Tokyo, Japan) equipped with a spinning disk confocal and TIRF combined system (Spectral Diskovery, Ontario, Canada). Two colour simultaneous TIRF laser illumination with 488 and 638 nm was provided by directly modulated lasers combined into a two fiber output (Spectral ILE, Ontario, Canada). Following the general methodology of O'Donoghue et al.[24], single molecule TIRFM measurements were imaged in streaming mode with a 500 ms exposure time to detect the bound fraction of ligand on the supported lipid bilayer. By using a 500 ms exposure, the bound ligands were detected as discrete spots of fluorescence intensity due to relatively slow diffusion of receptor-bound ligands; unbound ligands on the supported lipid diffused much faster and created a background blurred image on the camera detector (see Extended Data Figure 3a-b). Fluorescent emissions of GFP (receptor) and Atto647N (ligand) were split using a 650 nm long pass dichroic onto two Andor iXon Ultra EMCCDs (Belfast, Ireland). Illumination was controlled using digital control boards (Arduino Uno, Turin, Italy) and triggers from the cameras. Image acquisition was performed using MicroManager software[52]. A standard constant temperature of 37°C was maintained using an OKO Labs stage top incubator.

Single molecule diffraction limited spots in the far-red channel were detected and tracked using the FIJI plugin "Trackmate". Ligand dwell times, as computed from the track duration, were fit to a single exponential decay in Prism Graphpad software to calculate τ_{obs}, the mean observed dwell time. The dwell times for the four 11mer mutant oligonucleotides with increasing G/C content were tested on the one experimental day. Per each experiment, single molecule measurements were made from between 8-12 cells per DNA ligand. Bleach rates were determined by absorbing His10-CLIPf-ybbr13-Atto647N to clean glass imaged using identical illumination and acquisition conditions, and were obtained on the same day as ligand dwell time measurement. Bleaching data for single molecules was processed and analyzed in an identical manner to ligand dwell time data to determine the rate of bleaching (τ_{bl})(see also Extended Data Figure 3). τ_{obs} is a combination of the rate of dissociation and photobleaching,

and can be corrected to obtain τ_{corr} using the following formula:

$$\tau_{corr} = (\tau_{obs}^{-1} - \tau_{bl}^{-1})^{-1}$$

Imaging and Analysis of Single Ligand-Receptor Interactions and ZAP70 Recruitment

Imaging of ZAP70-GFP recruitment was performed on an inverted microscope (Nikon TiE, Tokyo, Japan) equipped with NIKON fiber launch TIRF illuminator. Illumination was controlled with an Agilent Laser combiner using the 488 and 640 nm laser lines at approximately 0.1 and 0.05 mW laser power respectively. Fluorescence emission was collected through filters for GFP (525 ± 25 nm) and Atto647N (700 ± 75 nm). All images were collected using a Nikon Plan Apo 100x 1.4 NA oil-immersion objective that projected onto a Photometrics Evolve EM-CCD camera with a calculated pixel size of 103 nm. A constant temperature of 37°C was maintained using a Tokai Hit stage top incubator.

JRT3 cells expressing DNA-CAR (under puromycin selection) and ZAP70-GFP were pipetted onto supported lipids bilayers functionalized with His10-CLIPf-Atto647N conjugated to DNA ligand. JRT3 cells and SLBs were sequentially illuminated for 500 ms with 488 nm and 640 nm laser lines. Diffraction-limited punctae of Atto647N representing bound DNA ligands were detected and tracked using Trackmate FIJI plugin as described above. A hidden Markov Model (HMM) analysis was then used to identify the number of fluorescent ligands in each frame from the fluorescent intensity of a tracked Atto647N ligand cluster. The same analysis was also used to detect the moment ZAP70 was recruitment to a DNA ligand microcluster. The HMM analysis implemented in this study was the statistical maximum evidence approach described previously by Bronson et al. (see Extended Data Fig. 4 and supplementary methods).

To analyze ligand on rate, we segmented the cells-SLB interface using the ZAP70-GFP fluorescence by applying a threshold using FIJI. We calculated the cell-SLB interface surface area from the thresholded image and using the Analyse Particle plugin, and calculated the median surface area during the initial 3 min of the cell landing on the SLB. We used this to calculate a ligand binding on-rate based on cell-SLB interface area and the number of de novo single molecule events detected in this 3 min window. We calculated the ligand on-rate in

clusters by scoring new binding events that occurred after the initial single molecule binding event that seeded that receptor-ligand cluster. The time interval was calculated from the molecule binding event that preceded the subsequent binding event (e.g the time interval between the second and third binding event). Micro-cluster area was estimated as a diffraction limit spot (calculated using a spot with 0.2 μm radius – radius^2 x π). We only analyzed events where clear quantal steps were detected. In most examples this meant we could reliably analyze the second and third ligand binding events, but in some case we could analyze up to 5 binding event at an individual micro-cluster.

Figures

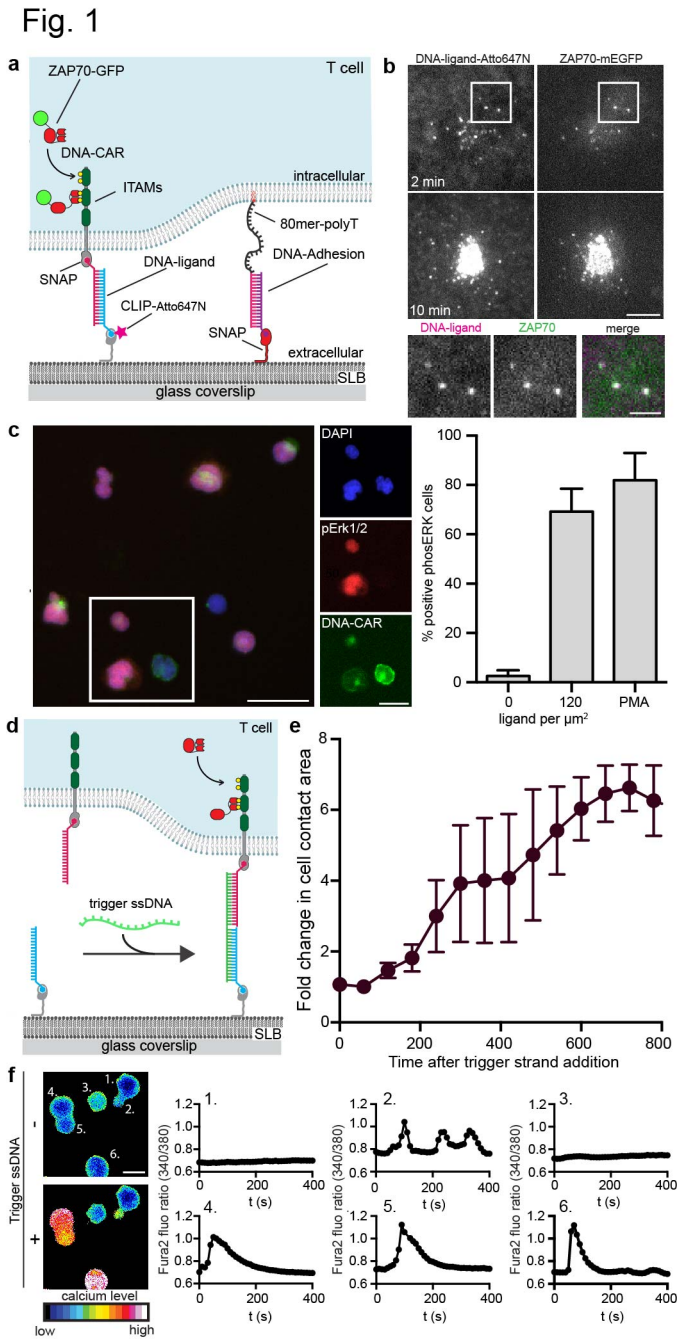

Figure 1. A DNA-CAR capable of triggering T cell signaling.

a. Schematic of the DNA-based chimeric antigen receptor system (DNA-CAR). The SNAPf tag and His10-CLIPf were covalently labeled with complementary strands of benzyl-guanine-DNA and benzyl-cytosine DNA respectively. Longer orthogonal DNA strands without

transmembrane coupling to an intracellular signaling domain were used to adhere cells to the bilayer without inducing signaling.

b. TIRF microscopy images of a JRT3 Jurkat cell expressing ZAP70-GFP and a CAR labeled with 16mer ssDNA after landing on a SLB with a complementary 16mer strand (120 molecules per μm^2). Microclusters of ligand-receptor complexes formed within ~2 min and recruited ZAP70-GFP (inset) and then moved centripetally and coalesced near the cell center at 10 min. Scale bar, 5 μm; inset scale bar, 2 μm.

c. To measure activation of the MAP kinase pathway, cells (15 min after SLB contact) were stained for phosphoERK (red); DAPI staining of nuclei (blue) and the DNA-CAR (green). Bar, 50 μm. Insert shows higher magnification of three cells. Inset bar, 20 μm. Quantification (see Extended Data Fig. 2, Methods) of the MAP kinase pathway activation by the 16mer DNA ligand compared to PMA (10 ng/ml). Mean ± s.d. of 6 experiments (>2500 cells scored per experiment).

d. A schematic of a triggerable DNA-CAR designed to examine temporal responses of T cell signaling. Although included in experiments, the adhesion strand shown in panel **a** is omitted for clarity.

e. Cell spreading on the SLB as a function of time after adding the DNA trigger strand. Plotted is average fold change in cell area as a function of time after addition of trigger strand. Mean ± s.e.m. from 3 separate experiments (3-7 cells analyzed per experiment).

f. Pseudo colour image of calcium level using the ratiometric Fura-2 calcium dye. Plots of the 340 nm/380 nm Fura-2 emission ratio showing the change in intracellular calcium levels from the six cells after adding the DNA trigger strand. Bar, 10 μm.

Fig. 2

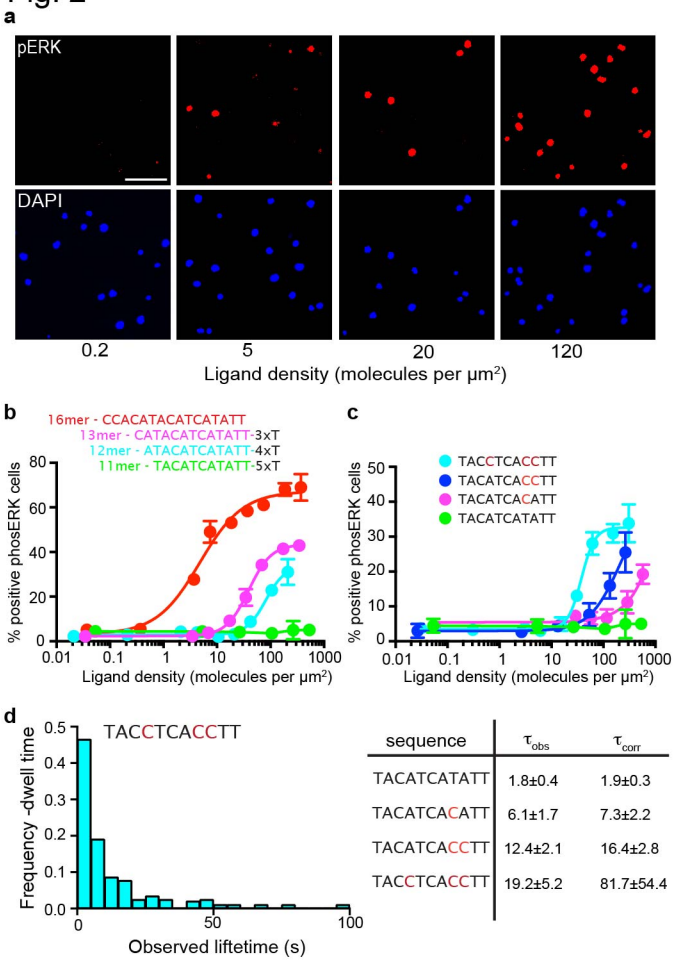

sequence	τ_{obs}	τ_{corr}
TACATCATATT	1.8±0.4	1.9±0.3
TACATCACATT	6.1±1.7	7.3±2.2
TACATCACCTT	12.4±2.1	16.4±2.8
TACCTCACCTT	19.2±5.2	81.7±54.4

Figure 2. Modulation of T-cell activation by DNA-CAR length and sequence.

a. PhophoERK staining of JRT3 cells responding to an increasing density of 16mer DNA ligand on SLBs (15 min). Threshold images are shown corresponding to the phosphERK staining and DAPI channel. Scale bar, 100 μm.

b. Dose response curves for DNA ligands of varying hybridization length. The total ligand DNA length remained constant by adding nonhybridizing Ts. Mean ± s.d. (n = 3).

c. Stepwise conversion of A/T to G/C base pairs increases the potency of the 11mer DNA ligand for inducing phosphoERK signaling. Scale bar, 100 μm. Each data point represents the mean ± s.d. from one experiment, where each ligand density was measured in triplicate. Data shown is representative of 3 independent experiments.

d. Measurement of the lifetime of single ligand-receptor interactions by TIRF microscopy. An example distribution of lifetimes from one DNA ligand. The observed (τ_{obs}) and photobleach-corrected (τ_{corr}) lifetimes are shown for the 11mer (mean ± s.e.m. from 3 separate experiments reported; for data of 13mer and 16mer and all histograms see Extended Data Fig. 3).

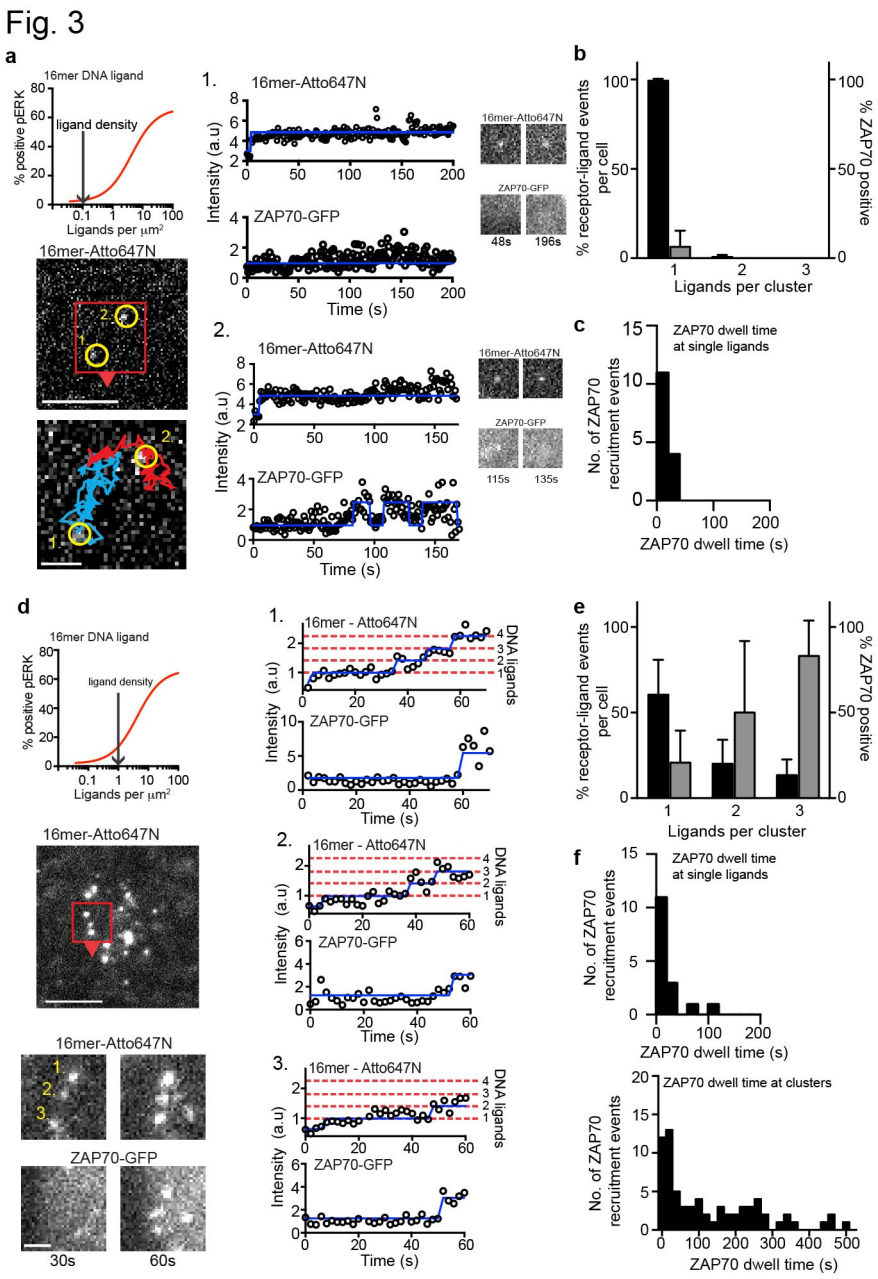

Figure 3. Receptor clustering increases the probability of ZAP70 recruitment.

Measuring ligand and ZAP70-GFP binding to DNA-CAR by TIRF imaging with a 16mer DNA ligand at 0.1 (a-c) and 1 ligand per μm² (d-e). Dose response curves shown in panel a and d are based on data shown in Fig. 2b. The blue line overlaid the Atto647N and ZAP70-GFP fluorescent intensity represents detected step changes in fluorescence intensity marking new ligand binding events or the recruitment of ZAP70. The dashed red lines mark the quantal ligand fluorescent intensities for a given number of DNA ligands, (determined using a hidden Markov model analysis; see Extended Data Figure 4 and Supplemental Information). Single or

multiple ligand binding events that persisted and could be followed for >30 s were scored for whether they recruited ZAP70-GFP. The initial point of ZAP70-GFP recruitment was referenced to the number of ligands within the receptor-ligand spot as in panel a and d.

a. TIRF images of 16mer DNA ligands labeled with Atto647N. Single bound ligands are marked by yellow circles in region of interest (red box and arrowhead). Bar, 5 μm. Right panel, region of interest overlaid with the tracked single molecule trajectories. ROI bar, 1 μm. Right panels, the fluorescent intensity time series for the 16mer ligand and the corresponding ZAP70-GFP fluorescent intensity. Ligand 1 in (a) shows a typical example of a bound ligand-receptor pair that does not recruit a ZAP70-GFP. Ligand 2 in (**a**) shows a less common example of ZAP70-GFP recruitment (often transient as shown here) to a single bound 16mer ligand.

b. Quantification of ZAP70-GFP recruitment at 0.1 ligand/μm^2 of 16mer DNA ligand. Bar plot shows the number single bound ligand-receptors and clusters (percent of total, black bars) and ZAP70 recruitment to ligand-receptors (percent of total that recruit ZAP70, grey bars). 6.3 ± 9% of single bound ligands that persist greater than 30 s recruit ZAP70. Results are mean ± s.d. from n = 9 cells.

c. Quantification of ZAP70 dwell time at single bound ligands of 16mer DNA ligand (n=15).

d. TIRF images of 16mer DNA ligands at 1 ligand/μm^2 (which elicits pERK signaling in ~20% of cells). Bar, 5 μm. Region of interest (red box and arrowhead) shows three ligand-receptor clusters (labeled 1-3). ROI bar, 1 μm. Fluorescent intensity time series from the DNA and ZAP70-GFP channels of the same 3 microclusters is shown on the right, For additional traces at various ligand densities, see Extended Data Fig. 5-6 and Movies S3-6.

e. Quantification of ZAP70 recruitment at 1 ligand/μm^2 of 16mer DNA ligand. Organization of bar plot same as shown (b). 83 ± 20% or receptor-ligand clusters composed of 3 or more ligands recruit ZAP70 versus 20 ± 18% of single bound receptors. Results are mean ± s.d. from n = 6 cells.

f. Distribution of ZAP70 dwell times at single bound receptors (n=16) and receptor-ligand clusters (n=70). For 32 of the clusters with ZAP70 dwells time of >100s, the measurement was truncated by the end of image acquisition.

Fig. 4

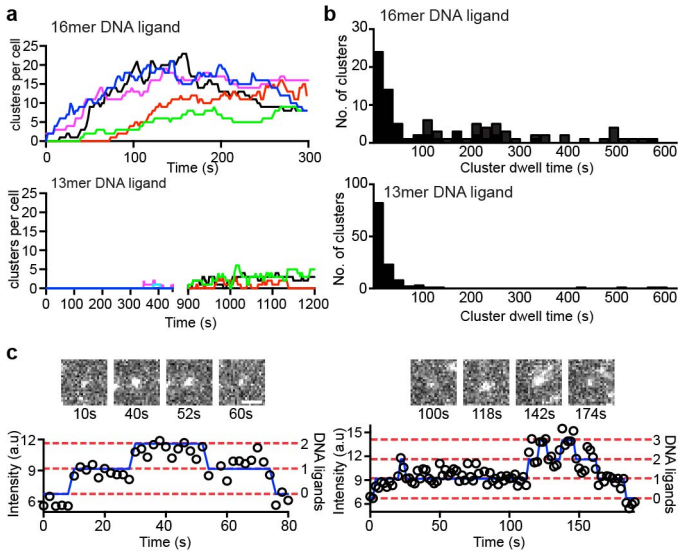

Figure 4. Difference in microcluster formation by low and high affinity ligands.

a. Formation over time of ligand-receptor clusters (defined as a diffraction limit structure containing 2 or more bound ligands) for individual cells (colors) between the 16mer and 13mer DNA ligand at a SLB density of 1 ligand/μm^2. For 16mer and 13mer plots at 0-15 min, t=0 is defined as the point of image acquisition, often within 1-2 min of application of cells to the SLB.

b. Distribution of dwell time for ligand-receptor clusters composed of 16mer (n=94 from 6 cells; 35 clusters with dwell times of >100 s and were truncated by the end of image acquisition) and 13mer DNA ligands (n=125 from 6 cells, 6 clusters with dwell times of >100 s were truncated by the end of image acquisition).

c. TIRF images and intensity time series showing the formation of transient receptor-ligand clusters of 13mer DNA ligand. The fluorescent time series were analyzed as described in Figure 3 and Extended Data Fig. 4.

Fig. 5

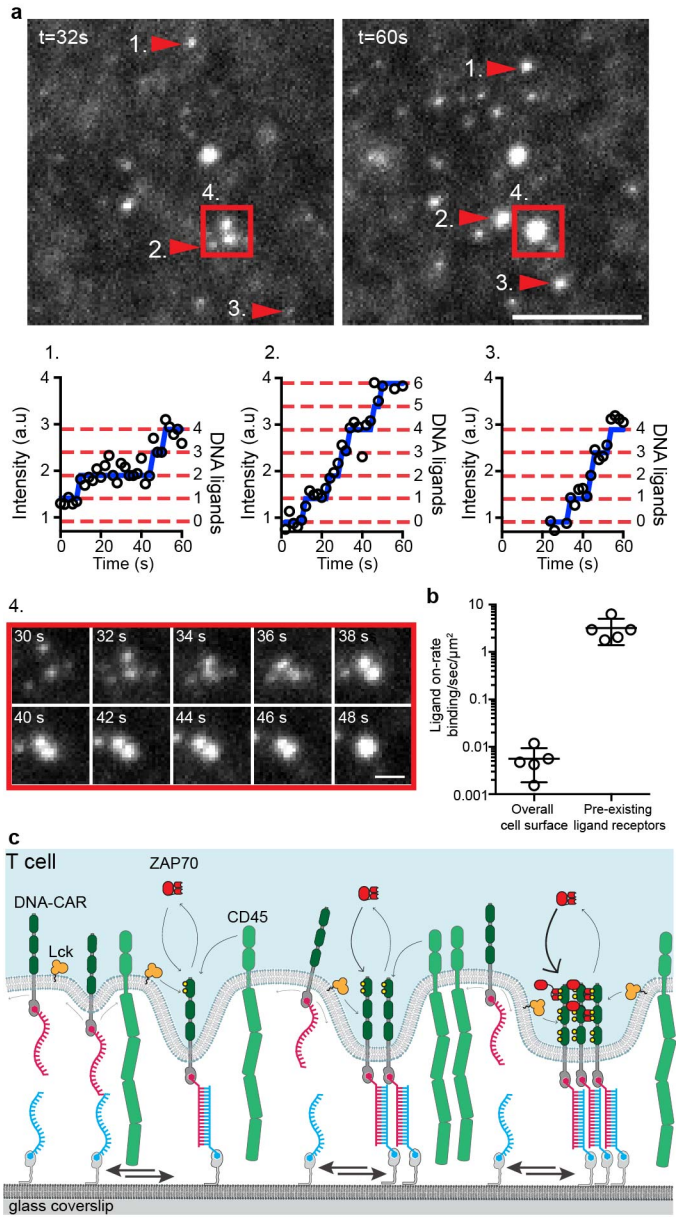

Figure 5. Formation of microclusters from single ligand-receptor binding events.

a. A TIRF image of receptor-bound 16mer DNA ligand organized into receptor-ligand clusters that grow by adjacent ligand binding events (red arrows numbered 1-3) and by merging and fusion (red box numbered 4). Bar, 2.5 μm. See Movie S7. Clusters grow by sequential addition of newly bound ligand; the blue line overlaid the fluorescent intensity represents detected step changes in fluorescence intensity (see methods and extended data Fig. 4). Time series (red box, numbered 4) below follows two receptor-ligand clusters (bar, 1 μm).

b. The rate of new ligand binding events near to an existing receptor-bound ligand (quantal increase in intensity in an existing diffraction-limited spot) or outside of these zones (measured by the sudden appearance of a new bound ligand in the contact area between the cell with the supported lipid bilayer). The ligand-receptor on-rate was expressed as the number of events per sec per μm^2 membrane surface area (using 0.126 μm^2 for a diffraction limited spot of a pre-existing ligand-receptor pair). Shown is the mean ± s.e.m. from 5 cells.

c. Model of how a single receptor-ligand binding event might nucleate receptor-ligand clusters and receptor phosphorylation. A single receptor-ligand interaction pins the two membranes in close apposition; unbound ligands that diffuse into this region are in closer proximity to and can more readily bind a receptor. Receptors in clusters more effectively exclude the phosphatase CD45, enabling their net phosphorylation by Lck. For lower affinity ligands, receptor clusters and phosphorylation can be reversed by ligand dissociation, providing a mechanism for kinetic proofreading (see text).

Extended Data

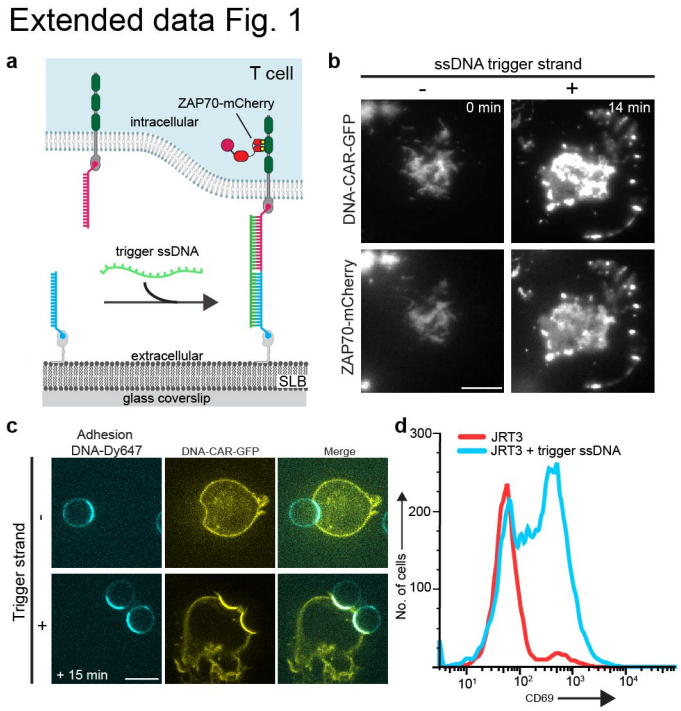

Extended Data Figure 1.

A triggerable DNA-CAR system induces formation of ZAP70 positive microclusters and CD69 cell surface expression.

a. A schematic of a triggerable DNA-CAR system with a 34 base pair overlap.

b. Formation of ZAP70-mCherry positive microclusters and cell spreading after addition of DNA trigger strand which results in an overlap of 35 bp. Bar, 5 μm. Time after addition of the trigger DNA strand is shown.

c. JRT3 cells expressing the DNA-CAR-GFP were mixed with 7 μm silica microspheres with adsorbed supported lipid bilayers functionalized with a DNA adhesion strand (in this example, conjugated to His10-SNAPf-ybbr13-Dy647) and DNA ligand (conjugated to His10-CLIPf)). SLB were set up on silica microsphere to maintain cells in suspension and facilitate FACS analysis. Cells and beads were mixed in a 96 well plate before the addition of the DNA trigger strand. To check SLB formation on silica beads as well as DNA-CAR activation, a portion of cells were plated onto poly-L-lysine coated coverslips and imaged by spinning disk confocal microscopy. Bilayer fluidity was checked by the enrichment of the His10-SNAPf-Dy647 at the cell-bead interface. 15 min after addition of trigger strand, the DNA-CAR-GFP is enriched at the cell-microsphere interface. Scale bar, 10 μm.

d. 4 hr after addition of trigger DNA strand, cells were stained for CD69 and analyzed by FACS. CD69 expression was upregulated on the cell surface for cells that were incubated with trigger strand (blue trace) compared with control cells (red trace).

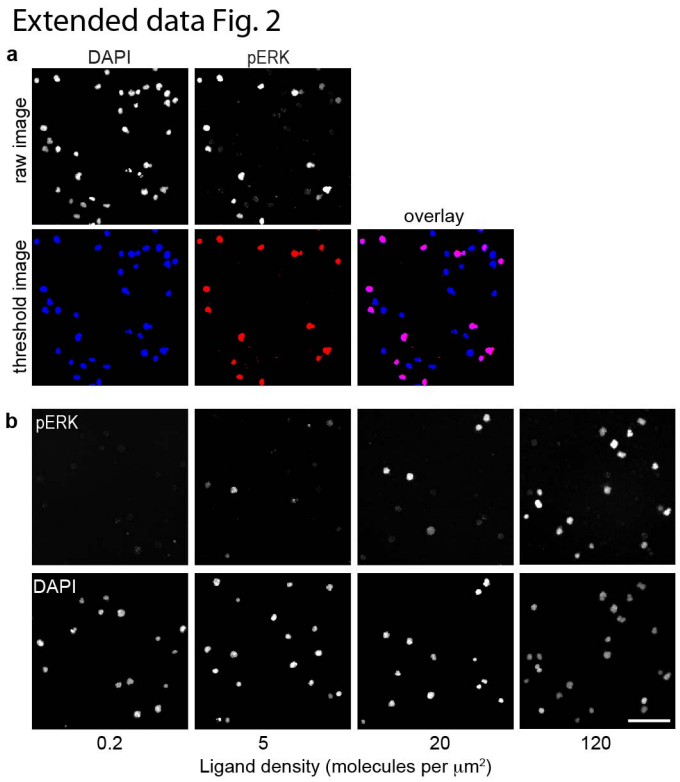

Extended Data Figure 2. PhosphoErk quantification.

a. A customized Cell Profiler analysis pipeline was used to process phosphoERK staining images and score JRT3 cells as phosphoERK positive or negative. First the DAPI channel raw images were segmented to identify the nucleus (shown as blue in the threshold image). Second the raw images of the phospoERK staining channeled were segmented using thresholding parameters set with control data sets (PMA stimulated cell, non-stimulated cells, and cells stained with secondary antibody only). Identified phosphoERK nuclei are shown as red in the thresholded image. Cells were scored phosphoERK positive when a DAPI nucleus overlapped with a segmented phosphoERK nucleus. A minimum threshold area was set for the nucleus as described in the Methods. In the overlay of the thresholded DAPI and phosphoERK images the nuclei scored positive appear magenta. Scale bar, 100 μm.

b. Raw and threshold phosphoErk and DAPI images presented in Fig 2a. Scale bar, 100 μm

Extended Data Fig. 3

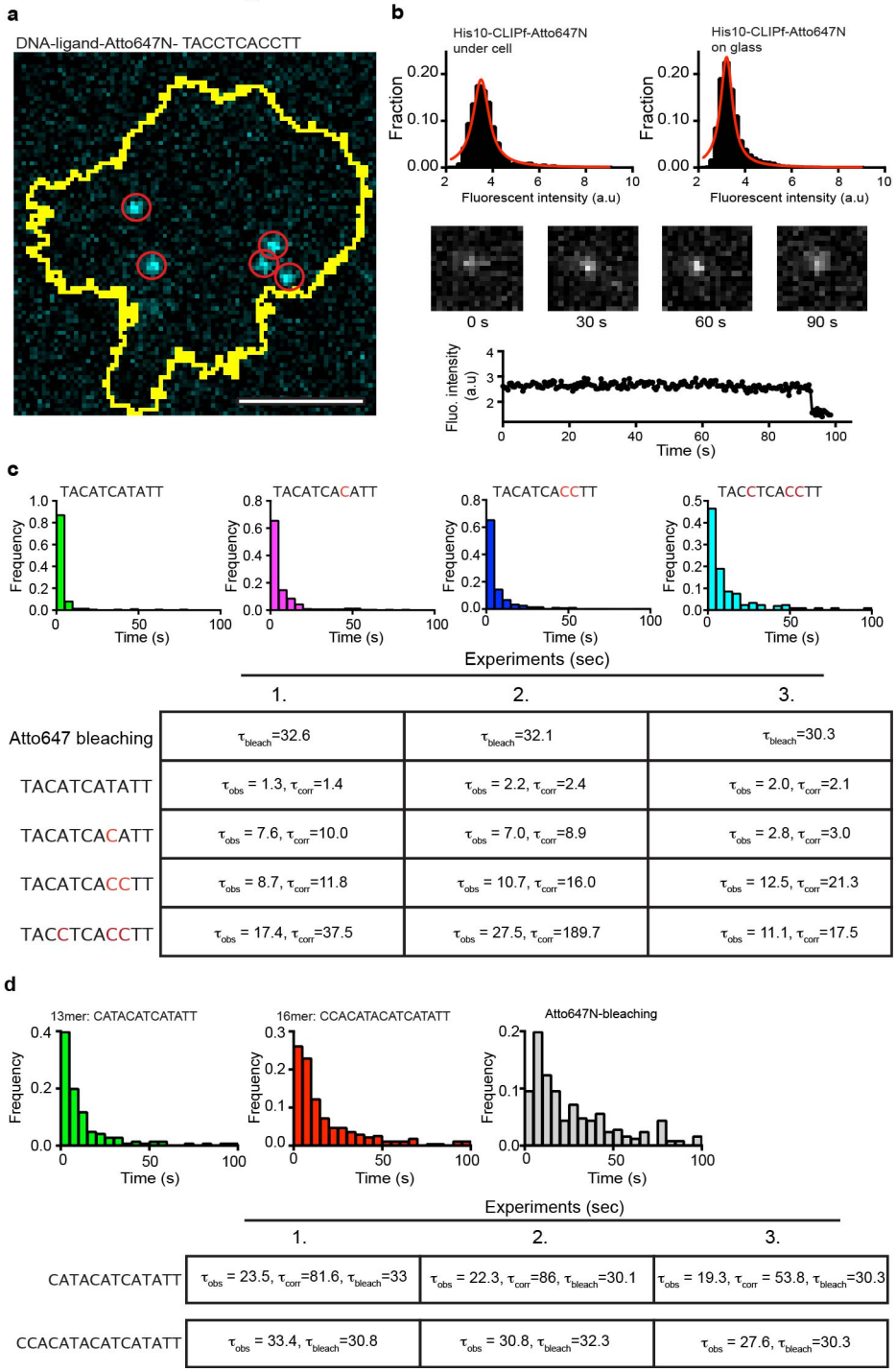

Extended Data Figure 3. Measuring receptor-ligand dwell time.

a. JRT3 cells expressing DNA-CAR were imaged using a two-camera TIRF microscope with simultaneous excitation of DNA-CAR-GFP and DNA-ligand-Atto647N. A long 500 ms exposure in the Atto647N channel revealed single molecules (red circles) of DNA-ligands-Atto647N

detected at the SLB-cell interface (yellow outline, obtained by segmentation using DNA-CAR-GFP fluorescence). In contrast to bound DNA ligand, unbound DNA ligands diffuse more rapidly and appear as a unresolved fluorescent blur in images taken at 500 ms exposure. (See method of O'Donoghue et al.[24]) Scale bar, 2.5 μm.

b. Top, mean fluorescent intensities of single receptor-bound DNA ligands versus single His10-CLIPf-ybbr labeled with Atto647N absorbed to glass and imaged with identical conditions. Bottom, representative intensity trace of a single receptor-bound DNA ligand labeled with Atto647N which is bound for 90 s, before disappearing by single step photobleaching/unbinding.

c-d. Histograms of dwell times for DNA ligand and tables of individual dwell times (τ_{obs}) and Atto647N bleaching measurements (τ_{bl}). Panel c shows the 3 experiments that make up the average dwell times presented in Fig. 2d for the 11mer DNA ligands. Each experiment for the 11mer ligand represents measurement conducted on one experimental day. A single experiment consisted of single molecule dwell times measurement from >10 cells with 300-700 single receptor ligand binding events per DNA ligand analyzed. Histograms of individual dwell time measurements for the 13mer and 16mer DNA ligand are presented in panel d. The τ_{obs} was corrected using the bleaching measurement performed during each experiment to obtain an estimate of average dwell time (τ_{corr}) of receptor ligand unbinding from:

$$\tau_{corr} = (\tau_{obs}^{-1} - \tau_{bl}^{-1})^{-1}$$

This method to estimate τ_{corr} is most accurate when τ_{obs} is considerably smaller that τ_{bl}. Measurements of τ_{obs} that approach τ_{bl} have an inflated τ_{corr}, as is the case the 11mer ligand with the greatest G/C content (AAGGTGAGGTA). In the case of the 16mer DNA ligand, τ_{obs} is equivalent to τ_{bl} making this correction method more prone to error.

Extended Data Fig. 4

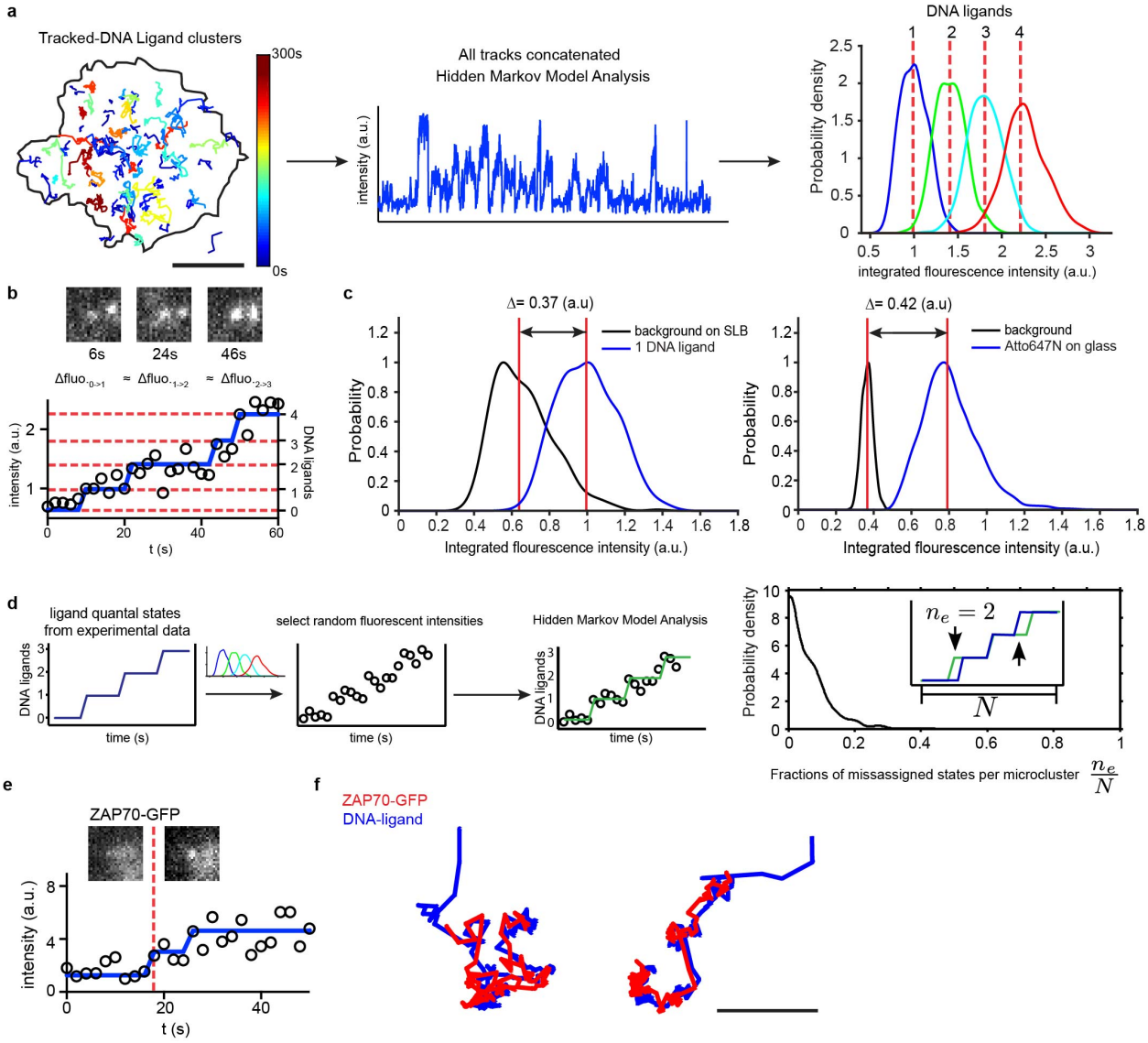

Extended Data Figure 4. Analysis of receptor-ligand microcluster formation and ZAP70 recruitment.

a. We adapted a previously described[53] Hidden Markov Model (HMM) analysis to identify the number of fluorescent ligands in each frame from the fluorescent intensity of tracked Atto647N ligand clusters. The intensity time-series of each tracked cluster was extracted from the coordinates generated by TrackMate. Shown is an example of 86 particle trajectories detected at the cell-SLB junction for the 16mer DNA ligand at ~1 molecule/μm^2 (black outline, segmented cell boundary; microcluster trajectories colour coded by lifetime). Bar, 5 μm. The intensity time-series of all tracks were then concatenated, and the ensemble intensity time

series was analyzed by a statistical maximum evidence approach, implemented with a variational Bayesian method. This analysis identified the rates of ligand addition and removal and the fluorescence distributions associated with n=1,2,3... bound ligands from the intensity data. We found the assigned distributions of fluorescent intensities are overlapping, as is expected from the highly fluctuating background noise generated by the fluorescent blur of the rapidly-diffusing unbound Atto647N-ligand on the camera detector. Nonetheless, each distribution shows a clear maximum and does not exhibit any structure indicative of misfitting (e.g. multiple peaks). Furthermore, the difference in the medians of each distribution peak is quantized, commensurate with the fluorescence intensity arising from a discrete numbers of fluorescent molecules. The identified rates and fluorescence distributions were used to reconstruct the time-series of ligand number for each cluster. This resulted in the identification of the step changes in the fluorescent signal that denoted new ligand binding events.

b. Example DNA ligand intensity time series overlaid with HMM-assigned ligand number at each time point (blue trace). The step changes in the blue trace represent the binding of new ligands. The dashed red lines represent the median fluorescent intensity from n=1,2,3… fluorescent ligands (derived from the fluorescence intensity distributions shown in panel a).

c. To ensure that the states identified by the HMM analysis corresponded to quantized intensity values characteristic of single molecules, we performed an identical analysis on data sets consisting of single Atto647N fluorophores stuck to glass slides. We then compared the fluorescent distributions of the n = 0 (i.e. background) and n = 1 fluorophore number with the distributions of the n=0 and n=1 fluorescent ligands found in the cell-bilayer data. We find that the difference in their medians is in good agreement (3.7 vs 4.2 fluorescent intensity units), confirming that the HMM analysis is reliably identifying states corresponding to discrete numbers of fluorescent molecules. We note that the HMM analysis was able to correctly identify states in both the stuck Atto647N dataset as well as the cell-based data-set despite the differences in noise between them (compare the distribution in the background on a SLB versus a glass slide). The background fluorescence intensity of the SLB was measured by sampling 5 time points previous to cluster appearance in a region of interest centered on the coordinate where the tracked microcluster appeared. The background distribution of the glass

slide was obtained by randomly sampling regions in the image stack not occupied by single molecules.

d. We assayed for the robustness of the HMM analysis to the broad fluorescence distributions by constructing a computer-generated data set. Time series of ligand binding and unbinding/bleaching were taken from an analyzed experimental dataset and converted into fluorescence values by sampling from the experimentally intensity distributions for n=1,2,3… DNA ligands shown in panel (a). This ensured that the noise and the transition rates between states in the computer-generated data set were reflective of experimentally collected data. The resultant time-series were analysed and the HMM reconstruction of state time series was compared to the original values. The error was quantified as the fraction of time-point in a time-series in which the HMM reconstruction misidentified the state. Plotting the distribution of error confirms that the algorithm is able to identify states with <10% error despite the noise present experimentally.

e. We used the algorithm described in (a) conservatively to assay for presence or absence of ZAP70. Due to the noisy background signal associated with the cytosolic ZAP70-GFP, we checked the HMM assignment of the first ZAP70-GFP binding event by manual visual inspection to determine whether the detected step change in intensity represented recruitment.

f. Representative DNA-ligand microclusters trajectories (blue) overlaid with the trajectory of an associated ZAP70-GFP spot (red). Positive ZAP70 recruitment was defined as a puncta of ZAP70-GFP that co-localized and co-migrated with an object in the ligand channel. By inspection of the data we found misidentified ZAP70 recruitment arose from two factors: 1) fluctuation in the Z-axis of the cell in the evanescent field, and 2) the presence of intracellular structures (likely endosomes) that were ZAP70-GFP positive that were prominent in some cells. These ZAP70-GFP punctae did not colocalise or move with ligand-bound receptors. Bar, 1 μm.

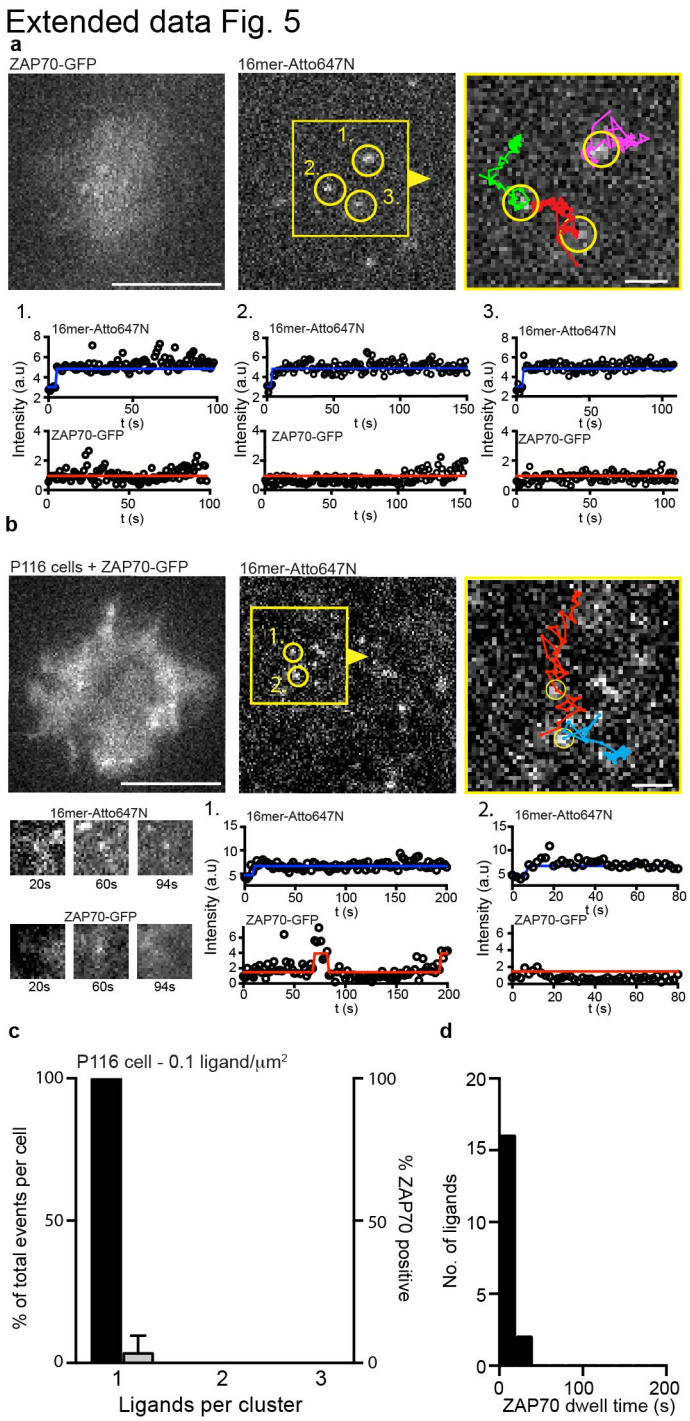

Extended Data Figure 5. Gallery of single molecule binding events in JRT3 and P116 (ZAP70-negative Jurkat cell line) expressing DNA-CAR and ZAP70-GFP.

Single molecule imaging was performed at a density 0.1 16mer-DNA ligands/ μm².

a. TIRF images of 16mer DNA ligands labeled with Atto647N. Single bound ligands are marked by yellow circles in region of interest (red box and arrowhead). Bar, 5 μm. Right panel, region

of interest overlaid with the tracked single molecule trajectories. ROI bar, 1 μm. Bottom panels, the fluorescent intensity time series for the single molecules of Atto647N labeled 16mer ligand and the corresponding ZAP70-GFP fluorescent intensity. Fluorescent intensity time series for ligand and ZAP70 channels analyzed as described in Extended Data Fig. 4.

b. TIRF images of a P116 cell expressing ZAP70-GFP and DNA-CAR. Bar, 5 μm. Region of interest (yellow box and arrowhead) on right overlaid with single molecule trajectories. ROI bar, 1 μm. Fluorescent intensity plots for bound ligands shown below images.

c. Quantification of ZAP70 recruitment to single bound receptors in P116 cells. Shown are the number single bound ligand-receptor pairs (percent of total, black bars) and the percent of single bound receptor and clusters that recruited ZAP70-GFP (grey bars) in P116 Jurkat cells. ZAP70 recruitment was only observed in 2.2 ± 4% of single molecules events in P116 cells. Results are mean ± s.d. from 6 P116 Jurkat cells.

d. Quantification of ZAP70 dwell time at single bound ligands of 16mer DNA ligand in P116 cells (n=18).

Extended Data Fig. 6

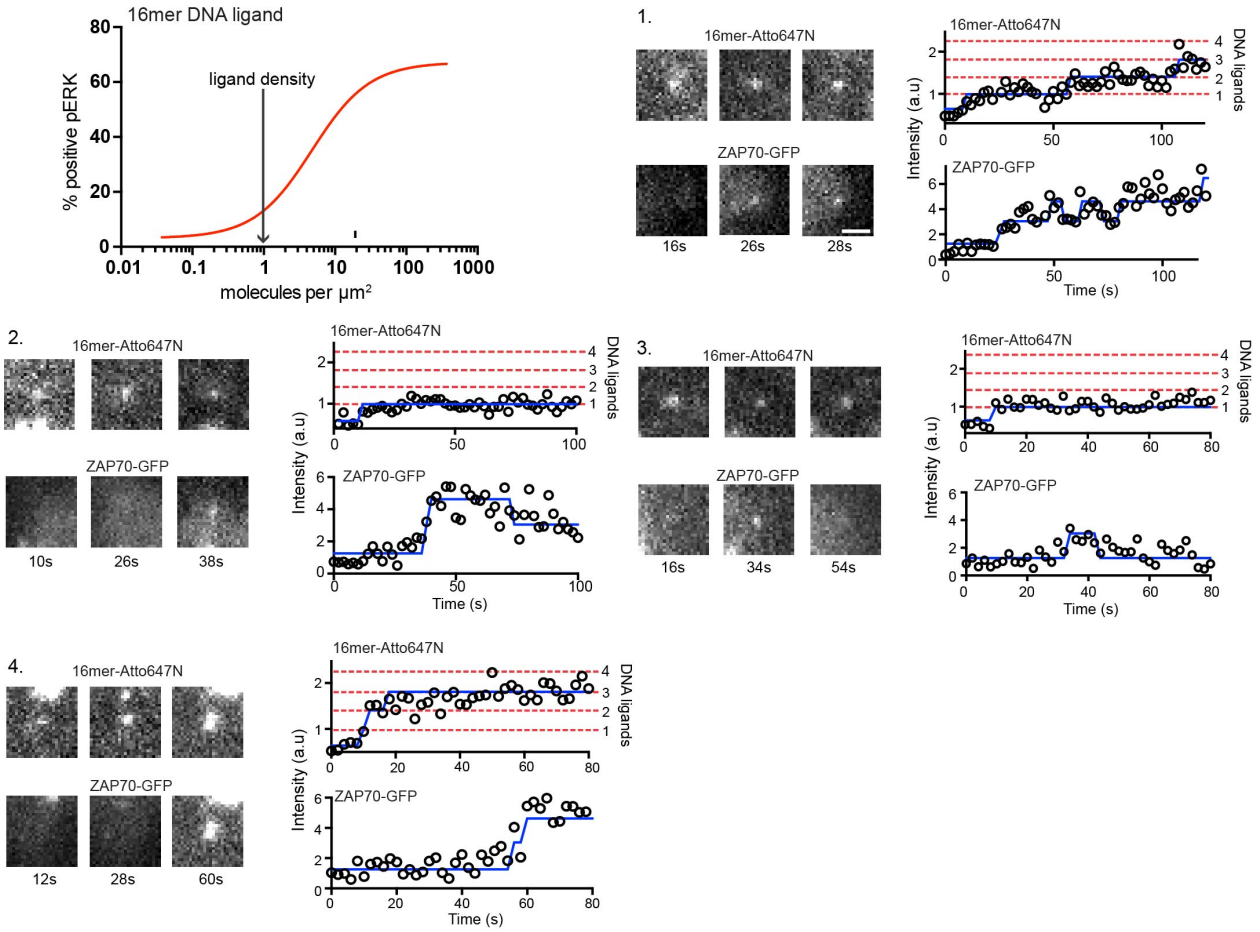

Extended Data Figure 6. Gallery of examples showing formation of receptor-ligand microclusters and ZAP70 recruitment to a high affinity 16mer DNA ligand.

Data shown were acquired by at a density of 1 ligand/μm². The DNA ligand and ZAP70 fluorescent intensity time series were analyzed as described in Extended Data Fig. 4.

a. Receptor-ligand microclusters of 16mer DNA-ligand that formed in the initial 5 min of interacting with the SLB. Although uncommon, ZAP70 recruitment was observed at single molecules of bound 16mer ligand (examples 1-3). In some cases ZAP70 recruitment to single bound 16mer ligands was transient (example 3). Receptor-ligand microclusters consisting of 2 or more 16mer DNA ligands (examples 4) were more likely to recruit ZAP70. Bar, 1 μm.

Extended Data Fig. 7

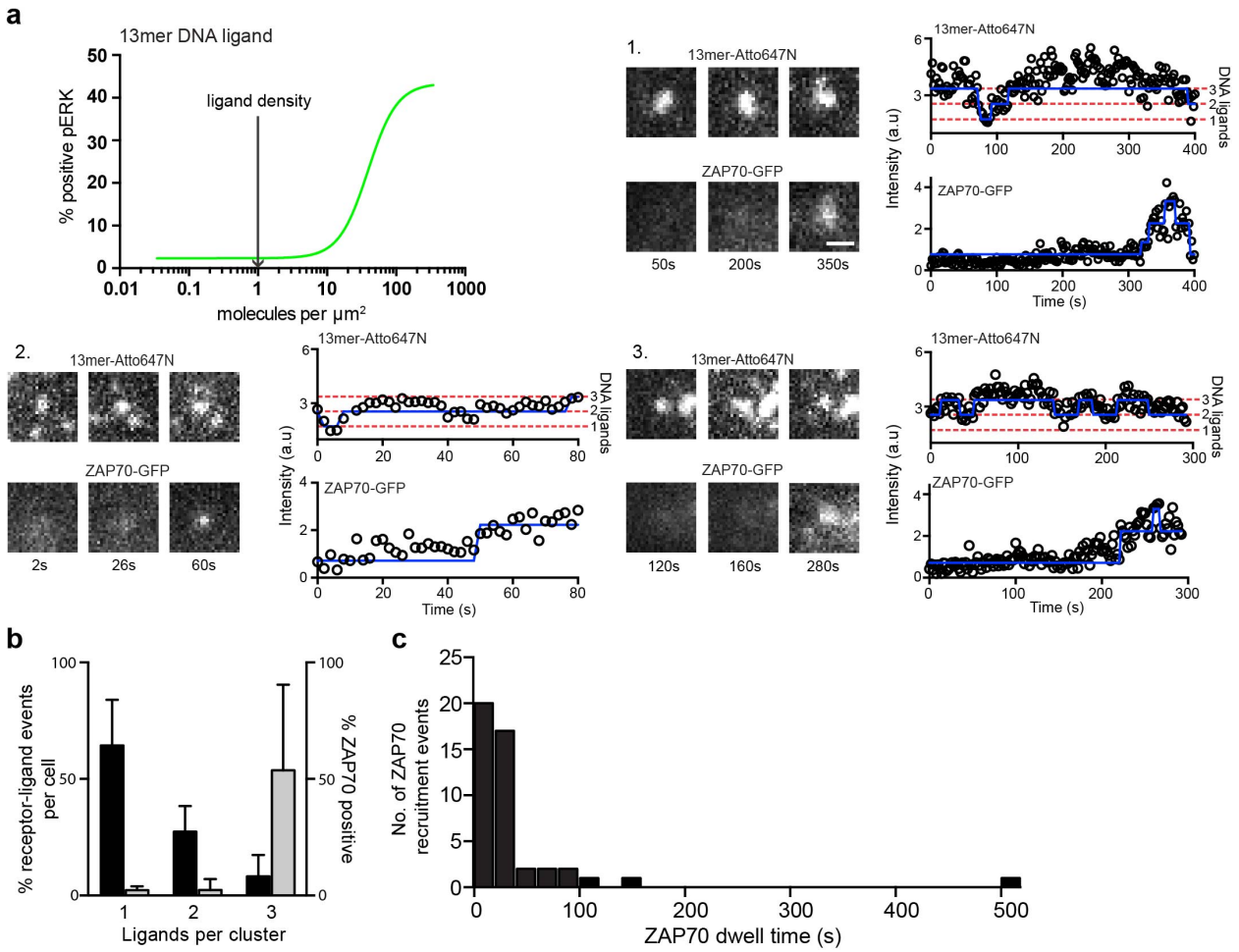

Extended Data Figure 7. Quantification and examples of receptor-ligand microclusters formation and ZAP70 recruitment to a low affinity 13mer DNA ligand.

Data shown acquired at a density of 1 ligand/µm². The DNA ligand and ZAP70 fluorescent intensity time series were analyzed as described in Extended Data Fig. 4.

a. A gallery of examples showing the formation of small receptor-ligand microclusters of 13mer DNA ligand observed after cells had interacted SLBs for >15 min.

b. Quantification of ZAP70 recruitment and dwell time to ligand-receptors of 13mer DNA ligand. Bar plot shows the number single bound ligand-receptor and clusters (percent of total binned, black bars) and quantification of (percent of total that recruit ZAP70, grey bars). Single molecule ligand binding events and receptor-ligand clusters of increasing ligand number that persisted for at least 30 s were scored for whether they recruited ZAP70-GFP. The initial point of ZAP70 recruitment was referenced to the number of ligands within the receptor-ligand spot.

53 ± 37% of receptor-ligand clusters containing 3 or more ligand recruit ZAP70 compared to 2 ± 1.7% of single bound ligands. Results are mean ± s.d. from n = 4 cells.

c. The distribution of ZAP70 dwell times at receptor-ligand clusters (n=46 cluster from 4 cells).

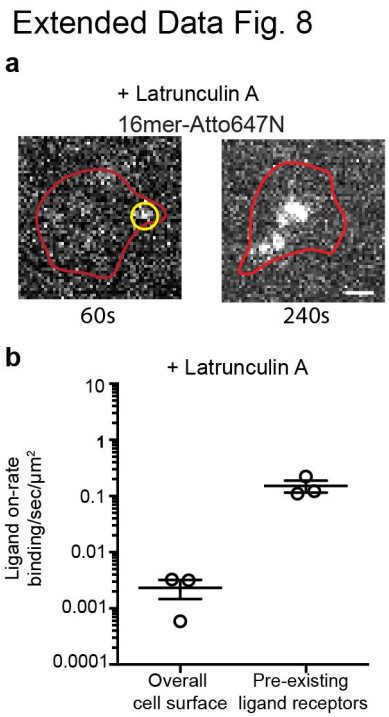

Extended Data Figure 8. Formation of DNA receptor ligand clusters in the presence of latrunculin A.

a. TIRF images showing cluster formation nucleated from a single bound receptor (yellow circle) in the presence of latrunculin A (1 μm) with a 16mer at 1 ligand/μm^2 (red outline show the cell outline obtained by segmentation using the ZAP70-GFP fluorescence). Bar, 1 μm.

b. The rate of new ligand binding events near to an existing receptor-bound ligand (quantal increase in intensity in an existing diffraction-limited spot) or outside of these zones (measured by the sudden appearance of a new bound ligand in the contact area between the cell with the supported lipid bilayer) in cell treated with latrunculin A (1 μm). The ligand-receptor on-rate was expressed as the number of events per sec per μm^2 membrane surface area (using 0.126 μm^2 for a diffraction limited spot of a pre-existing ligand-receptor pair). Shown is the mean ± s.e.m. from 3 cells.

References:

1. Davis, M. M. & Bjorkman, P. J. T-cell antigen receptor genes and T-cell recognition. *Nature* **334,** 395–402 (1988).
2. Davis, M. M. *et al.* Ligand recognition by alpha beta T cell receptors. *Annu. Rev. Immunol.* **16,** 523–544 (1998).
3. Feinerman, O., Germain, R. N. & Altan-Bonnet, G. Quantitative challenges in understanding ligand discrimination by alphabeta T cells. *Mol. Immunol.* **45,** 619–631 (2008).
4. Wallace, V. A., Penninger, J. & Mak, T. W. CD4, CD8 and tyrosine kinases in thymic selection. *Curr. Opin. Immunol.* **5,** 235–240 (1993).
5. Weiss, A. & Littman, D. R. Signal transduction by lymphocyte antigen receptors. *Cell* **76,** 263–274 (1994).
6. Irving, B. A. & Weiss, A. The cytoplasmic domain of the T cell receptor zeta chain is sufficient to couple to receptor-associated signal transduction pathways. *Cell* **64,** 891–901 (1991).
7. Sadelain, M., Brentjens, R. & Rivière, I. The basic principles of chimeric antigen receptor design. *Cancer Discov* **3,** 388–398 (2013).
8. SantaLucia, J. & Hicks, D. The thermodynamics of DNA structural motifs. *Annu Rev Biophys Biomol Struct* **33,** 415–440 (2004).
9. Gautier, A. *et al.* An Engineered Protein Tag for Multiprotein Labeling in Living Cells. *Chemistry & Biology* **15,** 128–136 (2008).
10. Ohashi, P. S. *et al.* Reconstitution of an active surface T3/T-cell antigen receptor by DNA transfer. *Nature* **316,** 606–609 (1985).
11. Mor, A. *et al.* The lymphocyte function-associated antigen-1 receptor costimulates plasma membrane Ras via phospholipase D2. *Nat. Cell Biol.* **9,** 713–719 (2007).
12. Selden, N. S. *et al.* Chemically programmed cell adhesion with membrane-anchored oligonucleotides. *J. Am. Chem. Soc.* **134,** 765–768 (2012).
13. Cantrell, D. T cell antigen receptor signal transduction pathways. *Annu. Rev. Immunol.* **14,** 259–274 (1996).
14. Smith-Garvin, J. E., Koretzky, G. A. & Jordan, M. S. T cell activation. *Annu. Rev. Immunol.* **27,** 591–619 (2009).
15. Zadeh, J. N. *et al.* NUPACK: Analysis and design of nucleic acid systems. *J Comput Chem* **32,** 170–173 (2011).
16. Varma, R., Campi, G., Yokosuka, T., Saito, T. & Dustin, M. L. T cell receptor-proximal signals are sustained in peripheral microclusters and terminated in the central supramolecular activation cluster. *Immunity* **25,** 117–127 (2006).
17. Kaizuka, Y., Douglass, A. D., Varma, R., Dustin, M. L. & Vale, R. D. Mechanisms for segregating T cell receptor and adhesion molecules during immunological synapse formation in Jurkat T cells. *Proc. Natl. Acad. Sci. U.S.A.* **104,** 20296–20301 (2007).
18. Grakoui, A. *et al.* The immunological synapse: a molecular machine controlling T cell activation. *Science* **285,** 221–227 (1999).
19. Stefanová, I. *et al.* TCR ligand discrimination is enforced by competing ERK positive and SHP-1 negative feedback pathways. *Nat Immunol* **4,** 248–254 (2003).
20. Kamentsky, L. *et al.* Improved structure, function and compatibility for CellProfiler: modular high-throughput image analysis software. *Bioinformatics* **27,** 1179–1180

(2011).
21. McKeithan, T. W. Kinetic proofreading in T-cell receptor signal transduction. *Proc. Natl. Acad. Sci. U.S.A.* **92,** 5042–5046 (1995).
22. Rabinowitz, J. D., Beeson, C., Lyons, D. S., Davis, M. M. & McConnell, H. M. Kinetic discrimination in T-cell activation. *Proc. Natl. Acad. Sci. U.S.A.* **93,** 1401–1405 (1996).
23. Lord, G. M., Lechler, R. I. & George, A. J. A kinetic differentiation model for the action of altered TCR ligands. *Immunol. Today* **20,** 33–39 (1999).
24. O'Donoghue, G. P., Pielak, R. M., Smoligovets, A. A., Lin, J. J. & Groves, J. T. Direct single molecule measurement of TCR triggering by agonist pMHC in living primary T cells. *Elife* **2,** e00778 (2013).
25. Chan, A. C., Iwashima, M., Turck, C. W. & Weiss, A. ZAP-70: a 70 kd protein-tyrosine kinase that associates with the TCR zeta chain. *Cell* **71,** 649–662 (1992).
26. Williams, B. L. *et al.* Genetic evidence for differential coupling of Syk family kinases to the T-cell receptor: reconstitution studies in a ZAP-70-deficient Jurkat T-cell line. *Mol. Cell. Biol.* **18,** 1388–1399 (1998).
27. Manz, B. N., Jackson, B. L., Petit, R. S., Dustin, M. L. & Groves, J. T-cell triggering thresholds are modulated by the number of antigen within individual T-cell receptor clusters. 1–6 (2011). doi:10.1073/pnas.1018771108/-/DCSupplemental/pnas.1018771108_SI.pdf
28. Huppa, J. B. *et al.* TCR-peptide-MHC interactions in situ show accelerated kinetics and increased affinity. *Nature* **463,** 963–967 (2010).
29. Gascoigne, N. R., Zal, T. & Alam, S. M. T-cell receptor binding kinetics in T-cell development and activation. *Expert reviews in molecular medicine* **2001,** 1–17 (2001).
30. Rabinowitz, J. D. *et al.* Altered T cell receptor ligands trigger a subset of early T cell signals. *Immunity* **5,** 125–135 (1996).
31. Klammt, C. *et al.* T cell receptor dwell times control the kinase activity of Zap70. *Nat Immunol* **16,** 961–969 (2015).
32. Krogsgaard, M. *et al.* Evidence that structural rearrangements and/or flexibility during TCR binding can contribute to T cell activation. *Mol. Cell* **12,** 1367–1378 (2003).
33. Schamel, W. W. A., Risueño, R. M., Minguet, S., Ortíz, A. R. & Alarcon, B. A conformation- and avidity-based proofreading mechanism for the TCR-CD3 complex. *Trends in Immunology* **27,** 176–182 (2006).
34. Li, Q.-J. *et al.* CD4 enhances T cell sensitivity to antigen by coordinating Lck accumulation at the immunological synapse. *Nat Immunol* **5,** 791–799 (2004).
35. Dushek, O. & van der Merwe, P. A. An induced rebinding model of antigen discrimination. *Trends in Immunology* **35,** 153–158 (2014).
36. Altan-Bonnet, G. & Germain, R. N. Modeling T cell antigen discrimination based on feedback control of digital ERK responses. *PLoS Biol.* **3,** e356 (2005).
37. Shaw, A. S. & Dustin, M. L. Making the T cell receptor go the distance: a topological view of T cell activation. *Immunity* **6,** 361–369 (1997).
38. James, J. R. & Vale, R. D. Biophysical mechanism of T-cell receptor triggering in a reconstituted system. *Nature* **487,** 64–69 (2012).
39. Qi, S. Y., Groves, J. T. & Chakraborty, A. K. Synaptic pattern formation during cellular recognition. *Proc. Natl. Acad. Sci. U.S.A.* **98,** 6548–6553 (2001).

40. Hu, J., Lipowsky, R. & Weikl, T. R. Binding constants of membrane-anchored receptors and ligands depend strongly on the nanoscale roughness of membranes. *Proc. Natl. Acad. Sci. U.S.A.* **110,** 15283–15288 (2013).
41. Davis, S. J. & van der Merwe, P. A. The kinetic-segregation model: TCR triggering and beyond. *Nat Immunol* **7,** 803–809 (2006).
42. Huang, J. *et al.* A single peptide-major histocompatibility complex ligand triggers digital cytokine secretion in CD4(+) T cells. *Immunity* **39,** 846–857 (2013).
43. Liu, B., Chen, W., Evavold, B. D. & Zhu, C. Accumulation of dynamic catch bonds between TCR and agonist peptide-MHC triggers T cell signaling. *Cell* **157,** 357–368 (2014).
44. Springer, T. A. Adhesion receptors of the immune system. *Nature* **346,** 425–434 (1990).
45. Chen, L. & Flies, D. B. Molecular mechanisms of T cell co-stimulation and co-inhibition. *Nature Publishing Group* **13,** 227–242 (2013).
46. Yin, J., Lin, A. J., Golan, D. E. & Walsh, C. T. Site-specific protein labeling by Sfp phosphopantetheinyl transferase. *Nat Protoc* **1,** 280–285 (2006).
47. Farlow, J. *et al.* Formation of targeted monovalent quantum dots by steric exclusion. *Nature Methods* **10,** 1203–1205 (2013).
48. Zhang, D. Y., Turberfield, A. J., Yurke, B. & Winfree, E. Engineering entropy-driven reactions and networks catalyzed by DNA. *Science* **318,** 1121–1125 (2007).
49. Douglass, E. F., Miller, C. J., Sparer, G., Shapiro, H. & Spiegel, D. A. A comprehensive mathematical model for three-body binding equilibria. *J. Am. Chem. Soc.* **135,** 6092–6099 (2013).
50. Chan, Y.-H. M., van Lengerich, B. & Boxer, S. G. Effects of linker sequences on vesicle fusion mediated by lipid-anchored DNA oligonucleotides. *Proc. Natl. Acad. Sci. U.S.A.* **106,** 979–984 (2009).
51. Schindelin, J. *et al.* Fiji: an open-source platform for biological-image analysis. *Nature Methods* **9,** 676–682 (2012).
52. Edelstein, A., Amodaj, N., Hoover, K., Vale, R. & Stuurman, N. Computer control of microscopes using µManager. *Curr Protoc Mol Biol* **Chapter 14,** Unit14.20 (2010).
53. Bronson, J. E., Fei, J., Hofman, J. M., Gonzalez, R. L. & Wiggins, C. H. Learning rates and states from biophysical time series: a Bayesian approach to model selection and single-molecule FRET data. *Biophys. J.* **97,** 3196–3205 (2009).

Supplemental Information

Generation of DNA-CARs and ZAP70 constructs

All oligonucleotides sequences used in cloning are listed in Supplementary Table 1 below. To construct DNA-CAR-GFP, the human CD3ζ cytoplasmic tails (a.a. 58-164) fused to the transmembrane domain of CD86 (a.a. 236-271) was amplified by polymerase chain reaction using primers MJT80/MJT81. The template used for this PCR was a CD86-CD3ζ chimeric receptor previously described[1]). Primers MJT80/MJT81 produced a DNA fragment with a 5' 3x gly-gly-ser linker and 3' BamH1 restriction site. A second PCR with primers MJT82/MJT83 amplified SNAPf (from the pSNAPf plasmid, New England Biolabs) with a N-terminal signal peptide (MQSGTHWRVLGLCLLSVGVWGQD) derived from CD3ε. Primers MJT82/MJT83 also introduced a 5' Mlu1 restriction site and 3' 3 x gly-gly-ser linker (complementary to the first PCR product). A stitch PCR was then set up with primers MJT80/MJT83. The final PCR product was digested with Mlu1 and BamH1 and ligated in frame with meGFP in the second-generation pHR-meGFP lentiviral vector.

DNA-CAR-IRESpuro was constructed with primers MJT134/MJT135 using DNA-CAR-GFP as PCR template. Forward primer MJT134 was designed so that a HA epitope tag was inserted between the signal peptide and the SNAPf open reading frame. This version of the DNA-CAR was digested with Mlu1 and BamH1 and ligated into a pHR lentiviral vector that had a downstream IRES-puromycin resistance cassette (pHR-DNA-CAR-IRES-puro). Apart from the addition of a HA tag or GFP in these two versions, the receptor was otherwise identical. All primers were purchased from Integrated DNA Technology, and primers longer that 60 nucleotides were ordered as Ultramer oligos.

Hidden Markov Model analysis of receptor-ligand cluster assembly and ZAP70 recruitment

The number of fluorescent ligands in a cluster is well described by a Markov process - that is, a stochastic process of ligand addition (i.e. the binding rate) and rates of ligand 'removal' (i.e. the combination of the unbinding and the bleaching rate). Therefore, we applied Hidden Markov Model methods to analyze the Atto647N channel data (as described in Extended Data Figure 4).

We implemented this analysis in Matlab by using the software vbFRET[2] (available at http://vbfret.sourceforge.net/ accessed on September 2015). First the intensity time-series of each tracked cluster was extracted from the coordinates generated by TrackMate. We also extracted the intensity values from the five frames that preceded the appearance of the object (to accurately sample background (i.e. no ligand) intensity values). The fluorescent intensity for each tracked microcluster from a cell was then concatenated to create an ensemble time series which was analysed by the vbFRET software package, which identified the rates of ligand binding and unbinding (or bleaching) and the fluorescence distributions for cluster composed of n=1,2,3… ligands. Finally vbFRET reconstructed the time-series of ligand number for each cluster using the Viterbi algorithm. We manually verified the reconstruction for every cluster in each cell, correcting for overfitting (i.e. the assigning of multiple Markov Model states to what is manually identifiable as a single fluorescent intensity state). To assay for the robustness of this analysis to experimental noise we used inverse transform sampling to re-noise a time-series of ligand number from an analyzed experimental dataset. This procedure randomly samples the fluorescent intensity distribution identified by vbFRET from the experimental data, and ensures the reconstructed data accurately reflects the experimental noise (Extended Data Figure 4d).

The same analysis protocol was implemented in the ZAP70 channel with minor differences (Extended Data Figure 4e). The tracking output of bound ligand coordinates was used to pull out the equivalent fluorescent intensity in the ZAP70-mEGFP channel using a custom written Matlab script. To aid analysis of the ZAP70-GFP signal, we analysed intensity values extracted from the ZAP70-GFP channel after a rolling ball background subtraction (performed in FIJI with ball size of 3 pixel) in parallel to the raw intensity values. HMM analysis of the ZAP70 data served as a guide for a subsequent careful manual analysis of the data. Manual verification was once again used to confirm positive recruitment as a puncta of ZAP70-GFP that co-localized and co-migrated with an object in the ligand channel (Extended Data Figure 4f).

Supplementary Table 1 Computational analysis of ssDNA binding free energy

Sequence:	ΔG(kcal/mol):
16mer AATATGATGTATGTGG	-15.85
13mer AATATGATGTATGttt	-12.16
12mer AATATGATGTATtttt	-10.73
11mer AATATGATGTAttttt	-10.14
11mers with increasing G/C content:	
AATGTGATGTAttttt	-11.86
AAGGTGATGTAttttt	-12.65
AAGGTGAGGTAttttt	-13.44

Calculated using nupack.org[3] (accessed on 06/12/2014). Input parameter were a temperature of 37° C with 150 mM NaCl and 2.5 mM $MgCl_2$.

Supplementary Table 2 Oligo sequences used to construct DNA-CARs

Construct	Oligo #	Sequence
DNA-CAR-GFP	MJT80	GGCGGAAGCGGAGGTAGTGGTGGAAGCCCCCCAGACCACATTCCTTGGATTACAG
	MJT81	gcgcggatcccgagggggcagggc
	MJT82	gcgcacgcgtgccgccaccatgcagtcgggcactcactggagagttctgggcctctgcctcttatcagttggcgtttgggggcaagatg aagactgcgaaatgaagcgc
	MJT83	GCGCGGATCCCGAGGGGGCAGGGCCTG
DNA-CAR-IRESpuro	MJT134	GCGCACGCGTGCCGCCACCATGCAGTCGGGCACTCACTGGAGAGTTCTGGGCCTCTGCCTCTTATCA TGGCGTTTGGGGGCAAGATTACCCATACGACGTCCCAGACTACGCTCTGCCCGAGACCGGCGGCGG GCGGCGGCGACAAAGACTGCGAAATGAAGCG
	MJT135	GCGCGGATCCTTACCGAGGGGGCAGGGCCT

Supplemental Movies Legends

Supplemental Movie 1. DNA-CAR forms dynamic microclusters that recruitment ZAP70

This video shows a JRT3 expressing DNA-CAR and ZAP70-GFP (green channel) interacting with a supported lipid bilayer functionalized with 120 molecules/μm^2 of 16mer DNA ligand-Atto647N (magenta channel). Video illustrates that the DNA-CAR forms dynamic microclusters when engaged with a complementary DNA strand ligand, and DNA-CAR microclusters recruit ZAP70 and move from the cell periphery to coalesce under the cell. Same cell as shown in Fig. 1b. Scale bar, 5 μm.

Supplemental Movie 2. Calcium flux in JRT3 activated by an inducible DNA-CAR.

JRT3 cells loaded with the Fura2 calcium dye were activated using an inducible DNA-CAR, as described in Fig. 1d. Shown is the pseudo-color video of the Fura 2 emission ratio (340/380 nm excitation). The Fura 2 emission ration is constant until the addition of trigger strand at 200 s results cytosolic flux of calcium in a portion of cells at ~260 s. Scale bar, 5 μm.

Supplemental Movie 3. Single molecule imaging of bound DNA ligands and ZAP70

Video showing single molecules of 16mer DNA ligand (magenta channel, bilayer density of 0.1 molecules/μm2) detected at the bilayer-cell interface of a JRT3 cell expressing DNA-CAR and ZAP70-GFP (green channel). Single bound 16mer DNA ligands (labeled with atto647N) are detected as described in Extended data Fig. 3. Despite the long lifetime of the DNA-CAR-16mer interaction, ZAP70-GFP recruitment is rarely seen at single ligand engaged receptors. Same cell as shown in Fig. 3a. Scale bar, 1 μm.

Supplemental Movie 4. Monitoring the assembly of DNA-CAR-ligand microclusters and ZAP70 recruitment .

This video shows a JRT3 expressing DNA-CAR and ZAP70-GFP (green channel) interacting with a SLB functionalized 16mer DNA ligand labeled with atto647N (magenta channel, ligand density 1 molecules/μm^2). At this ligand density the initial moment in the formation of small receptor-ligand microclusters can be detected. This movie shows that brighter receptor-ligand microclusters (consisting of 3 or more DNA ligands) more readily recruit ZAP70. Same cell as shown in Fig 3d. Scale bar, 1 μm.

Supplemental Movie 5. A weaker 13mer DNA ligand and ZAP70 recruitment.

Video showing a JRT3 expressing DNA-CAR and ZAP70-GFP (green channel) in in the initial minutes (<15 min after been after been applied to the bilayer) of interacting with a SLB functionalized 13mer DNA ligand labeled with atto647N (magenta channel, ligand density 1 molecules/μm2). In contrast to an equivalent density of the 16mer ligand, the majority of bound 13mer ligands are short lived and do not recruit ZAP70. Scale bar, 1 μm.

Supplemental Movie 6. Receptor ligand microclusters of 13mer DNA ligand are more readily observed in cells after 15 mins.

Video of a JRT3 cell after 15 min on a bilayer functionalized with 1 molecules/μm2 of 13mer DNA ligand (magenta channel). Microclusters of 13mer ligand were more readily observed after cell had been incubated with supported lipid bilayers for longer time period (>15 min, Fig. 4a). ZAP70 recruitment (green channel) was almost exclusively observed a microclusters consisting of 3 or more DNA ligands. Examples of DNA microclusters and ZAP70 recruitment from this cell are shown in extended data Fig. 7. Scale bar, 1 μm.

Supplemental Movie 7. Receptor ligand microcluster primarily assemble by the addition of newly bound ligand

Video of JRT3 interacting with a bilayer functionalized with 1 molecules/μm2 of 16mer DNA ligand (same cell as shown in Fig 5a). This video illustrates how microclusters primarily assemble by the unitary addition of newly bound ligand. The blue, red, and green overlays in the ligand channel (magenta) correspond to microclusters 1-3 shown in Fig. 5a. The ZAP70 channel is shown in green. Scale bar, 1 μm.

References

1. James, J. R. & Vale, R. D. Biophysical mechanism of T-cell receptor triggering in a reconstituted system. *Nature* **487,** 64–69 (2012).
2. Bronson, J. E., Fei, J., Hofman, J. M., Gonzalez, R. L. & Wiggins, C. H. Learning rates and states from biophysical time series: a Bayesian approach to model selection and single-molecule FRET data. *Biophys. J.* **97,** 3196–3205 (2009).
3. Zadeh, J. N. *et al.* NUPACK: Analysis and design of nucleic acid systems. *J Comput Chem* **32,** 170–173 (2011).